International Journal of Biological Macromolecules

Dye Degradation, Antibacterial Activity and Molecular Docking Analysis of Cellulose/Polyvinylpyrrolidone-doped Cadmium sulphide Quantum dots

--Manuscript Draft--

Manuscript Number:	IJBIOMAC-D-22-02883R2
Article Type:	Research Paper
Section/Category:	Carbohydrates, Natural Polyacids and Lignins
Keywords:	Quantum Dots; Co-precipitation; catalytic activity
Corresponding Author:	Muhammad Ikram Government College University Lahore Department of Physics Lahore, Pakistan PAKISTAN
First Author:	Aqsa Rafique
Order of Authors:	Aqsa Rafique
	Muhammad Ikram
	Ali Haider
	Anwar Ul-Hamid
	Sadia Naz
	Walid Nabgan
	Junaid Haider
	Iram Shahzadi
Abstract:	In present study, control sized cadmium sulphide (CdS) quantum dots (QDs) and cellulose nanocrystals grafted polyvinylpyrrolidone (CNC-g-PVP) doped CdS QDs were synthesized via co-precipitation. The suggested pathway is fruitful in throwing out organic pollutants like methylene blue (MB) from industrial water and bactericidal applications. A series of characterization techniques were used to determine the structural, optical and morphological qualities of prepared samples. The X-ray diffraction (XRD) pattern verified hexagonal structure with no significant change occurring in the spectrum upon doping (2, 4, and 6%). The UV-vis spectrophotometer describes blueshift in absorption pattern, resulting in an increase in band gap energy (E_g) upon doping. Catalytic activity (CA) against MB in basic and neutral medium demonstrated remarkable results compared with the acidic medium. Furthermore, bactericidal potential of doped sample (6%) exhibited the significantly higher inhibition zones of 5.25 mm and 4.05 mm against Staphylococcus aureus (S. aureus) or Gram-positive (G + ve) and Escherichia coli (E. coli) or Gram-negative (G-ve) , respectively. In silico predictions for these doped QDs were performed against selected enzyme targets (i.e. DNA gyrase and FabI) to unveil the mystery governing these bactericidal activities.
Suggested Reviewers:	Dayong Wu dayongwu@mail.ipc.ac.cn
	Qasim Khan qasim@szu.edu.cn
	Muhammad Maqbool mmaqbool@uab.edu
Opposed Reviewers:	
Response to Reviewers:	Reviewer #3: This manuscript deals with an interesting work on dye degradation, antibacterial activity and molecular docking analysis of cellulose/polyvinylpyrrolidone-doped cadmium sulphide quantum dot. Different methods including XRD, FTIR, UV-vis spectroscopy, PL, HRTEM, SAED, FESEM and EDS were used to characterize the as-synthesized nanostructures. Experimental results indicated that the catalytic activity (CA) against methylene blue (MB) in basic and neutral medium demonstrated

	remarkable results compared with the acidic medium. Furthermore, bactericidal potential of doped sample (6%) exhibited the significantly higher inhibition zones of 5.25 mm and 4.05 mm against S. aureus and E. coli, respectively. In silico predictions for these doped QDs were performed against selected enzyme targets (i.e. DNA gyrase and FabI) to unveil the mystery governing these bactericidal activities. Specific comments: 1. All abbreviations should be defined at the first usage. Please carefully check them throughout the text. Ans: According to recommendations, all abbreviations are defined at the first use. 2. Metal sulphides are popular, having unique applications as semiconductors, catalysts, solar radiation absorbers, cathodic materials, polymer surface coatings and nanoscale size switches. Recent works on the metal sulphides (e.g., CdS:Mn quantum dot-functionalized g-C3N4 nanohybrids as signal-generation tags for photoelectrochemical immunoassay of prostate specific antigen coupling DNAzyme concatamer with enzymatic biocatalytic precipitation; Exciton-plasmon interaction between AuNPs/graphene nanohybrids and CdS QDs/TiO2 for photoelectrochemical aptasensing of prostate-specific antigen; Near-infrared light-excited core-core-shell UCNP@Au@CdS upconversion nanospheres for ultrasensitive photoelectrochemical enzyme immunoassay; Palindromic Molecular Beacon-Based Z-Scheme BiOCl-Au-CdS Photoelectrochemical Biodetection) should be mentioned for this description. Meanwhile, the advantages of metal sulphides should be further discussed in the introduction. Ans: All the suggested research articles are incorporated in the manuscript, and further the benefits of metal sulphides also discussed. (Page 3) 3. CdS has an intrinsic optical band gap energy of 2.42 eV, absorption coefficient (104-105 cm−1), refractive index (2.5), mobility (0.1-10 cm2 V−1 S−1) and higher chemical stability, which makes it useful in catalysis, microelectronics, optoelectronics, photovoltaics, non-linear optics, photoelectrochemistry and also in other domains. Please provide the corresponding literatures! Actually, literatures on the CdS are insufficient. Ans: The corresponding literature added as well as the CdS characteristics was discussed. (Page 3) 4. The mechanism on dye degradation, antibacterial activity and molecular docking analysis of cellulose/polyvinylpyrrolidone-doped cadmium sulphide quantum dot should be further discussed and explained in the main text. Ans: Dye degradation, antibacterial and molecular docking analysis mechanisms have been explained in manuscript text as per recommendations respectively at (Pages 17-18, 22 and 23) 5. Table 3 on current and reported studies of CdS antibacterial activity might be removed to the Supporting Information. Ans: Table 3 removed to supporting information 6. Please carefully check all references, and irrelative references should be removed. Meanwhile, old literatures should be updated, especially before 10 years. Ans: As per recommendation old references have been updated.

Dear Editor and Referees:

We are very thankful to the reviewers for the critical assessment of our manuscript IJBIOMAC-D-22-02883 . Keeping in view their critique, we have made careful modifications to the original manuscript. All corrections are marked in the revised manuscript and the explanation to the reviewers' comments are listed in a separate "Answers to the reviewers' comments" document. We believe that the manuscript has been greatly improved and hope it has reached your Journal's standard.

Sincerely,

Dr. Muhammad Ikram

Solar Cell Applications Research Lab, Department of Physics,

G. C. University Lahore, Punjab Pakistan

Author Statement

Aqsa Rafique- Writing - original draft

Muhammad Ikram- Conceptualization, Data curation, Supervision, Funding acquisition

Ali Haider- Data curation, Writing – review & editing.

Anwar Ul-Hamid – Resources, Writing – review & editing.

Sadia Naz- Software

Walid Nabgan- Investigation, Formal analysis

Junaid Haider – Validation, Methodology

Iram Shahzadi -Formal analysis

Reviewer #3: This manuscript deals with an interesting work on dye degradation, antibacterial activity and molecular docking analysis of cellulose/polyvinylpyrrolidone-doped cadmium sulphide quantum dot. Different methods including XRD, FTIR, UV-vis spectroscopy, PL, HRTEM, SAED, FESEM and EDS were used to characterize the as-synthesized nanostructures. Experimental results indicated that the catalytic activity (CA) against methylene blue (MB) in basic and neutral medium demonstrated remarkable results compared with the acidic medium. Furthermore, bactericidal potential of doped sample (6%) exhibited the significantly higher inhibition zones of 5.25 mm and 4.05 mm against S. aureus and E. coli, respectively. In silico predictions for these doped QDs were performed against selected enzyme targets (i.e. DNA gyrase and FabI) to unveil the mystery governing these bactericidal activities.
Specific comments:

1. All abbreviations should be defined at the first usage. Please carefully check them throughout the text.

Ans: According to recommendations, all abbreviations are defined at the first use.

2. Metal sulphides are popular, having unique applications as semiconductors, catalysts, solar radiation absorbers, cathodic materials, polymer surface coatings and nanoscale size switches. Recent works on the metal sulphides (e.g., CdS:Mn quantum dot-functionalized g-C3N4 nanohybrids as signal-generation tags for photoelectrochemical immunoassay of prostate specific antigen coupling DNAzyme concatamer with enzymatic biocatalytic precipitation; Exciton-plasmon interaction between AuNPs/graphene nanohybrids and CdS QDs/TiO2 for photoelectrochemical aptasensing of prostate-specific antigen; Near-infrared light-excited core-core-shell UCNP@Au@CdS upconversion nanospheres for ultrasensitive photoelectrochemical enzyme immunoassay; Palindromic Molecular Beacon-Based Z-Scheme BiOCl-Au-CdS Photoelectrochemical Biodetection) should be mentioned for this description. Meanwhile, the advantages of metal sulphides should be further discussed in the introduction.

Ans: All the suggested research articles are incorporated in the manuscript, and further the benefits of metal sulphides also discussed. (Page 3)

3. CdS has an intrinsic optical band gap energy of 2.42 eV, absorption coefficient (104-105 cm−1), refractive index (2.5), mobility (0.1-10 cm2 V−1 S−1) and higher chemical stability, which makes it useful in catalysis, microelectronics, optoelectronics, photovoltaics, non-linear optics, photoelectrochemistry and also in other domains. Please provide the corresponding literatures! Actually, literatures on the CdS are insufficient.

Ans: The corresponding literature added as well as the CdS characteristics was discussed. (Page 3)

4. The mechanism on dye degradation, antibacterial activity and molecular docking analysis of cellulose/polyvinylpyrrolidone-doped cadmium sulphide quantum dot should be further discussed and explained in the main text.

Ans: Dye degradation, antibacterial and molecular docking analysis mechanisms have been explained in manuscript text as per recommendations respectively at (Pages 17-18, 22 and 23)

5. Table 3 on current and reported studies of CdS antibacterial activity might be removed to the Supporting Information.

Ans: Table 3 removed to supporting information

6. Please carefully check all references, and irrelative references should be removed. Meanwhile, old literatures should be updated, especially before 10 years.

Ans: As per recommendation old references have been updated.

Dye Degradation, Antibacterial Activity and Molecular Docking Analysis of Cellulose/Polyvinylpyrrolidone-doped Cadmium sulphide Quantum dots

Aqsa Rafique[a], Muhammad Ikram[a], Ali Haider[b], Anwar Ul-Hamid[c], Sadia Naz[d], Walid Nabgan[e], Junaid Haider[d], Iram Shahzadi[f]

[a]Solar Cell Applications Research Lab, Department of Physics, Government College University Lahore, Lahore, 54000, Punjab, Pakistan

[b]Department of Clinical Sciences, Faculty of Veterinary and Animal Sciences, Muhammad Nawaz Shareef, University of Agriculture, 66000, Multan, Punjab, Pakistan

[c]Core Research Facilities, King Fahd University of Petroleum & Minerals, Dhahran, 31261, Saudi Arabia

[d]Tianjin Institute of Industrial Biotechnology, Chinese Academy of Sciences, Tianjin 300308, China

[e]Departament d'Enginyeria Química, Universitat Rovira i Virgili, Av Països Catalans 26, 43007, Tarragona, Spain.

[f]Punjab University College of Pharmacy, University of the Punjab, Lahore, 54000, Pakistan

Corresponding Authors Email: [a]dr.muhammadikram@gcu.edu.pk, [c]anwar@kfupm.edu.sa, [e]wnabgan@gmail.com

ABSTRACT

In present study, control sized cadmium sulphide (CdS) quantum dots (QDs) and cellulose nanocrystals grafted polyvinylpyrrolidone (CNC-g-PVP) doped CdS QDs were synthesized via co-precipitation. The suggested pathway is fruitful in throwing out organic pollutants like methylene blue (MB) from industrial water and bactericidal applications. A series of characterization techniques were used to determine the structural, optical and morphological qualities of prepared samples. The X-ray diffraction (XRD) pattern verified hexagonal structure with no significant change occurring in the spectrum upon doping (2, 4, and 6%). The UV-vis

spectrophotometer describes blueshift in absorption pattern, resulting in an increase in band gap energy (E_g) upon doping. Catalytic activity (CA) against MB in basic and neutral medium demonstrated remarkable results compared with the acidic medium. Furthermore, bactericidal potential of doped sample (6%) exhibited the significantly higher inhibition zones of 5.25 mm and 4.05 mm against Staphylococcus aureus (*S. aureus*) or Gram-positive (G_+ve) *and* Escherichia coli (*E. coli*) or Gram-negative (G-ve), respectively. *In silico* predictions for these doped QDs were performed against selected enzyme targets (i.e. DNA gyrase and FabI) to unveil the mystery governing these bactericidal activities.

Keywords: Quantum dots; co-precipitation; catalytic activity

1. INTRODUCTION

Water is an essential component of life and has a crucial role in industry and economic development on the Earth. Additionally, growing human activities and rapid industrial growth result in the discharge of numerous injurious inorganic and organic contaminants (heavy metals and dyes, etc.) into the water, which endangers freshwater resources and the ecological environment (1, 2). Dyes are classified into three kinds anionic, cationic, and nonionic. Anionic dyes are separated into direct or acid, whereas cationic dyes are termed as basic dyes. MB is a cationic dye used in industrial sector to produce wood, paper, leather, silk etc. (3). Annually about 1/10th million different dyes were manufactured; among these, approximately 10–15% of MB is emitted directly into the surrounding environment, and water bodies cause serious environmental problems with higher chemical oxygen demand for aquatic life (4, 5). Environmental nanotechnology is critical in developing unique, straightforward, environmentally promising, and cost-favorable approaches for detecting, degrading, removing dangerous organic and inorganic contaminants (6). Numerous routes of ozonation (7), membrane filtration (8), adsorption (9) and catalytic reduction (10, 11) have been used to address this particular issue. Catalysis is considered environmentally beneficial, economically viable, energy-efficient, and has exceptional efficacy in completely oxidizing and mineralizing hazardous organics (12, 13). Mastitis is the most general production illness in the dairy sector worldwide (14). It is a mammary gland irritation that manifests as chemical, bacteriological and physical changes in milk (15, 16). Several factors, including host, the season, environment, farm management and specific agent pathogens such as *S. aureus* and *E. coli* can cause it (14, 17).

Metal sulphides (MSs) are semiconducting compounds in which sulphur is an anion linked to a metal cation, and metal ions can be mono-, bi-, or multi-form. The wider array of available MSs provides a unique platform for the construction of a large number of potential materials exhibiting exotic chemical, physical, and electronic phenomena, as well as novel functional properties and applications (18). The diverse class of MSs semiconductor materials that exhibit excellent optical properties, such as quantum confinement, and are used as QDs in fields as imaging, photocatalysis, and solar cells (19). MSs are popular, having unique applications as semiconductors (20), catalysts (21), solar radiation absorbers, cathodic materials (22), polymer surface coatings and nanoscale size switches (23-25) Semiconductor nanomaterials have recently gained popularity due to photoreactivity and catalytic properties (26). The transition metal sulphides are CuS, Ag_2S, FeS_2, CdS, and ZnS; among these, CdS has an intrinsic optical Eg of 2.42 eV, absorption coefficient (10^4–10^5 cm^{-1}), refractive index (2.5), mobility (0.1–10 cm^2 V^{-1} S^{-1}) and higher chemical stability, which makes it useful in catalysis (27), microelectronics (28), optoelectronics (29), photovoltaics (30), non-linear optics (31), photoelectrochemistry (32, 33) and, also as window layer in solar cells (34) and in other domains (35, 36). CdS is a binary chemical that is affordable, easily accessible, and effective. CdS has a limited number of surface trapping states, making it effective for electrical and optical applications (37). Due to the fact that it possesses n-type semi conductivity, it is utilized in heterojunction solar cells as a partner for p-type material (38). Cadmium is an electrically conductive, corrosion-resistant transition metal. CdS QDs are fluorescent semiconducting colloidal crystals. CdS NPs or QDs have outstanding optical and electrical properties and may be used in a range of applications (39). It also functions as a fluorescent material due to excellent semiconducting properties; its use in nucleic acid determination is well documented (40). Three CdS crystalline phases are hexagonal (wurtzite), cubic (zinc blende), and high-pressure rock salt. Hexagonal and cubic phases are distinguished by atomic arrangement. Wurtzite occurs in bulk and nanocrystalline in all three phases, but cubic and rock-salt only in nanocrystalline. Wurtzite CdS has been studied more than zinc-blende CdS since it's more stable and easily synthesised (41, 42). Several techniques have been adopted to prepare CdS with different sizes and shapes, e.g., chemical bath deposition, spray pyrolysis, laser deposition, sol-gel and successive ion layer adsorption (27). The co-precipitation technique is facile, economical, and single-step (43).

However, the formation of large CdS particles decreased surface area due to aggregation and increased exciton recombination rate (44).

To address this challenge, an amorphous polymer polyvinylpyrrolidone (PVP) is considered helpful in controlling the shape and size of QDs. PVP is a hydrophilic polymer having high solubility in polar solvents (water), non-toxic, non-ionic, high environmental stability, secure processability and good charge transfer capacity (45-47). Cellulose nanocrystals (CNCs) are crystalline in nature and insoluble fiber, having nano-sized rod-like morphologies widely employed in regenerated biosources, self-healing materials, membranes, thin films, and nanocomposites. The mechanical strength and adsorption ability improved and boosted the number of surface functional groups, particularly OH groups, by converting cellulose to nanoscale structures (47-49). High CNC content and amorphous (polymer matrix) components provided a mimetic approach for research to avoid CNC agglomeration (47). The hydroxyl group presence in CNCs enables the fabrication of composites, including polar, hydrophilic polymers PVP. CNC and PVP have modest molecular interactions and may interact via bound water. However, electrospun fibers made of CNC-g-PVP show no antibacterial properties (47, 50).

In current study, we added CNC-g-PVP into CdS to form CNC-g-PVP doped CdS QDs by co-precipitation pathway. The influence of as-prepared and doped samples on MB degradation and bactericidal action against *S. aureus* and *E. coli* were studied. Additionally, dopant impact on CdS morphological, structural, optical and chemical composition was examined and addressed. Although PVP conjugates with nanoparticles have been previously reported as good bactericidal agents, however, a clear mechanism is yet unknown. *In silico* molecular docking predictions of CNC-g-PVP and CNC-g-PVP doped CdS were performed against two attractive targets, i.e. DNA gyrase and FabI, for antibiotics discovery to clear the mystery governing these activities.

2-EXPERIMENTAL SECTION

2.1. Materials

Cadmium Chloride .2,5-hydrate ($CdCl_2$. $2,5H_2O$, 98%) was bought from PRS, Thiourea (CH_4N_2S, 99%), Avicel® pH-101 (~50 μm particle size), polyvinylpyrrolidone (PVP, Mw 40,000), sodium hydroxide (NaOH, 98%), and ammonia solution (33%) were purchased from Sigma Aldrich (Germany). Sulfuric acid (H_2SO_4) was attained from Analar (USA).

2.2. Synthesis of CNC and CNC-g-PVP dopants

To prepare CNCs, 10 g avicel was dispersed in 64% of H_2SO_4 and stirred at 75 °C for 45 min. H_2SO_4 dilution was attained by putting 20-fold of DI water into a yellow-brownish mixture under vigorously stirring. Generated precipitates were collected by centrifugation at 7500 rpm for 15 min and washed several times until a neutral solution was acquired and adjusted pH using an aqueous NaOH (0.3 M) solution. To obtain the powder, CNCs were dried at 105 °C.

The co-precipitation technique was used to make CNC-g-PVP composites. 0.5 g PVP was dissolved in DI water and stirred for 2 hours at room temperature. The CNC-g-PVP ratio was adjusted by introducing CNC stoichiometrically in a predetermined amount of stirring solution and vigorously stirring for 1 hour. Moreover, NaOH solution was poured to adjust the pH~12 and dried at 150 °C to get a product that was ground to attain fine powder (47). A proposed schematic illustration of synthesized CNC and CNC-g-PVP is shown in Fig. 1(a).

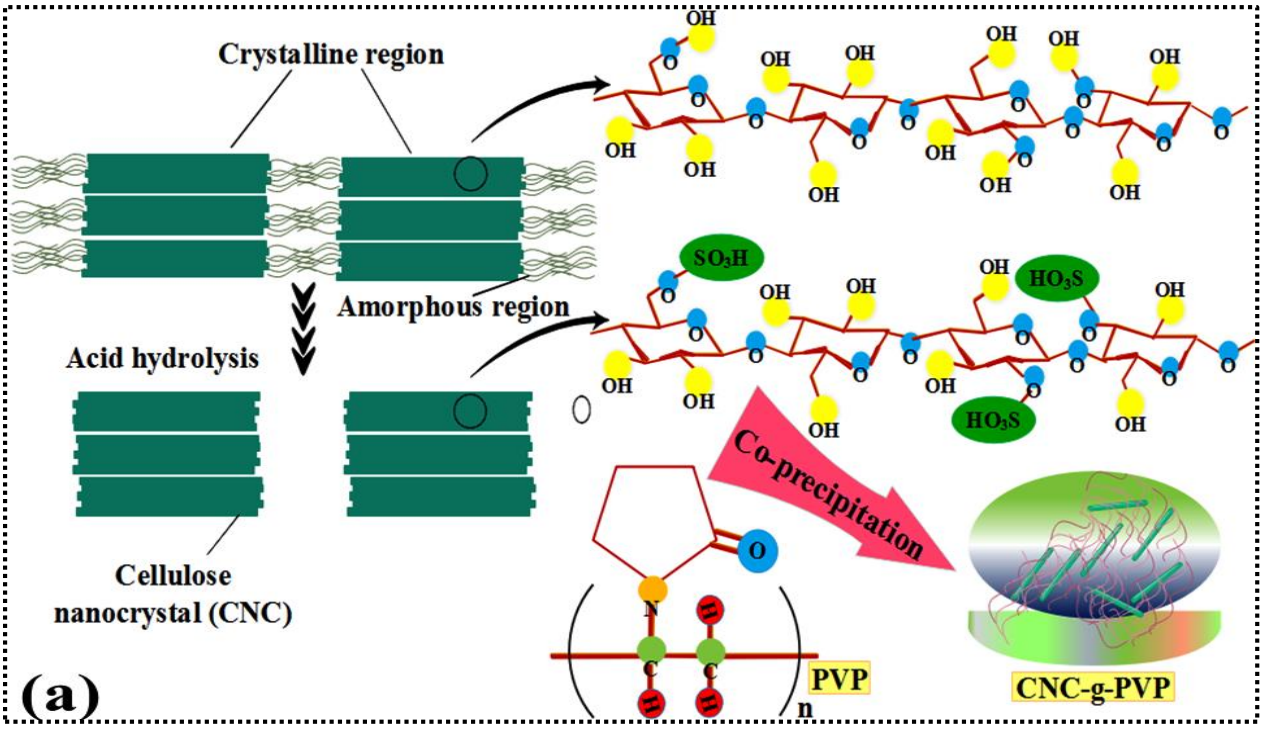

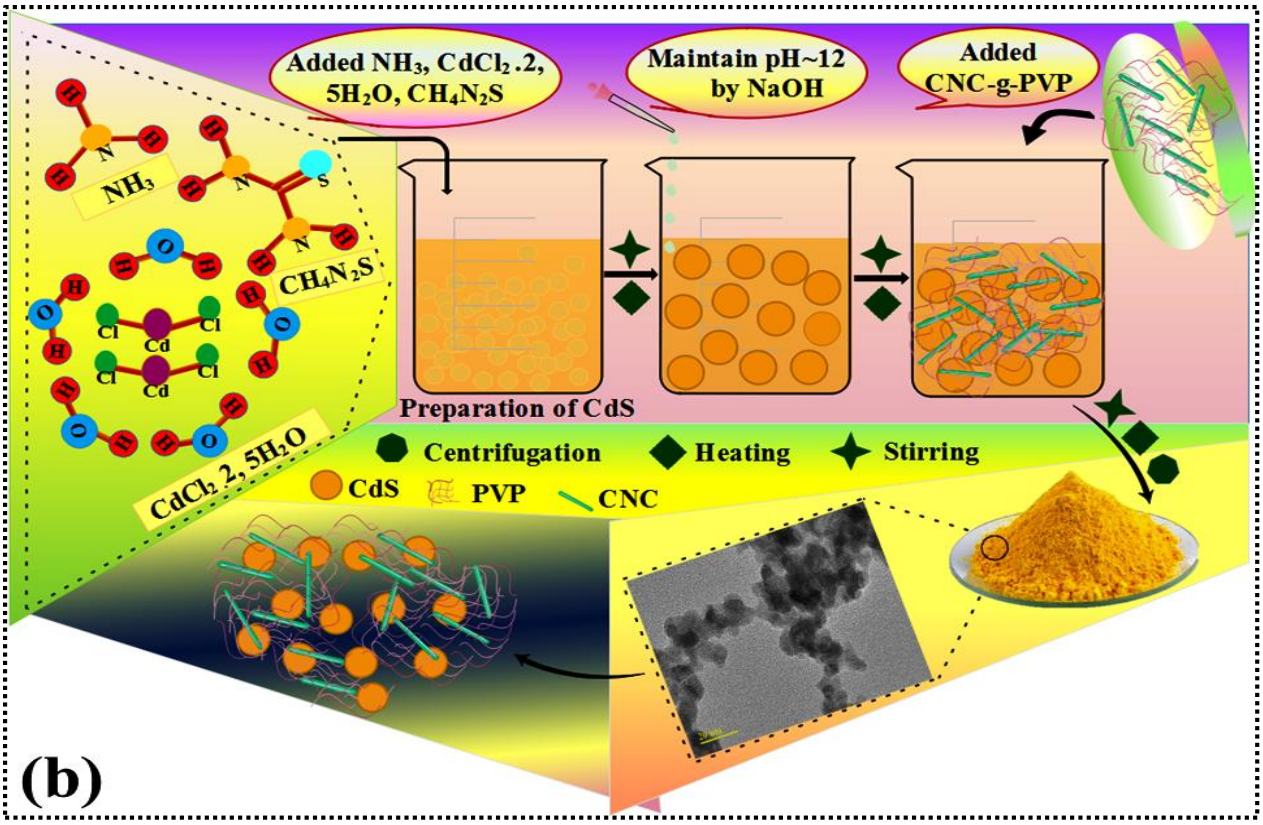

Fig. 1. (a) Acid hydrolysis process schematic illustration to synthesize CNC and CNC-g-PVP synthesis by co-precipitation, (b) Schematic illustration for synthesis process of CNC-g-PVP doped CdS QDs

2.3 Synthesis of CdS QDs and CNC-g-PVP doped CdS QDs

To synthesize CdS QDs co-precipitation pathway was adopted; initially, 0.2 M solution of ($CdCl_2$ .2,$5H_2O$) and 0.2 M of (CH_4N_2S) were mixed and stirred for 30 min at 80 °C. Subsequently, NaOH was incorporated drop wise to maintain pH~12 into the agitated solution. The precipitation process began and desired amount of NH_3 solution was added into pH maintained solution under the stirring for a further 10 min. Then precipitates were harvested by centrifugation at 7500 rpm for 6 and washed twice with DI water to remove contamination. Harvested sample was dried for 12 h at 150 °C to attain fine powder. CNC-g-PVP doped CdS was prepared by adding various amounts of CNC-g-PVP (0, 2, 4, and 6%) to achieve the weight ratio of CNC-g-PVP to CdS (0:1, 0.02:1, 0.04:1, and 0.06:1, respectively) and revising the above procedure to obtain the effects of dopants on CdS. Fig. 1(b) shows a schematic representation of the synthesis process.

2.4 Catalysis

Freshly synthesized (400 µL) solution of $NaBH_4$ was mixed with 3 mL aqueous MB solution (10 ppm) and absorption spectra detected after specified intervals. Afterwards, 400 µL of samples like CdS, CNC-g-PVP, and CNC-g-PVP with varied concentrations of doped CdS were added under agitation. The degradation was observed at regular intervals using a wavelength range of 200-800 nm by UV-vis spectrophotometer.

2.5 Isolation of *Staphylococcus aureus* and *E*scherichia *coli*

Caprine and bovine mastitic milk samples have been collected from various Punjab farms and initially cultured at 5% blood agar. The samples were incubated at 37 °C for 24 hours, resulting in, distinct colonies were streaked on mannitol salt agar (MSA) and MacConkey agar (MA) in triplets to isolate purified *S. aureus* and *E. coli*. The morphological and biochemical confirmation proceeded through catalase and coagulase tests and Gram's staining technique.

2.6 Antibacterial activity

Antimicrobial activity describes a condition in which an active substance reduces the viability of microorganisms. Gram-negative (G-ve) *E. coli* and Gram-positive (G_+ve) *S. aureus* bacteria insulated from caprine as well as bovine mastitis were used to evaluate the antibacterial properties of CNC-g-PVP doped CdS QDs. Ager well diffusion test was used to assess in vitro antibacterial efficacy by culturing *S. aureus* and *E. coli* isolates on MSA and MA plates. Bacterial solutions comprising 1.5×10^8 CFU ml^{-1} (0.5 Mc-Farland standards) were swabbed on petri dishes, and wells with a diameter of 6 mm were made using a sterile cork borer. Under aseptic conditions, different concentrations of prepared samples (500 µg/50 µl) and (1000 µg/50 µl) were poured into each well and compared with ciprofloxacin (5 µg/50 µl) and DI water (50 µl) as positive and negative controls, separately. The inhibition areas recovered after 24 hours of incubation were quantitatively measured through vernier caliper.

2.6.1 Statistical Analysis

The measured inhibition regions were statistically compared with controls using one-way variance analysis by SPSS version 22.

2.7 Molecular docking studies:

The role of PVP as a drug delivery agent and its importance in the pharmaceutical industry is well documented (51). Literature revealed the good antimicrobial potential of PVP conjugated nanomaterials (52, 53). Keeping in view the good antibacterial activity of CNC-g-PVP doped CdS QDs, in this study, molecular docking studies were performed for in-depth analysis and rationalize the possible mechanism. Structural coordinates for DNA gyrase and FabI enzymes from *E. coli* and *S. aureus*, respectively, were attained from a repository of protein crystal structures (https://www.rcsb.org/). The accession codes used for DNA gyrase$_{E.\ coli}$ and FabI$_{S.\ aureus}$ were 6KZZ (54) and 4CV1 (55), respectively.

Molecular docking predictions were performed using ICM Molsoft version 3.8-7d (Molsoft L.L.C., La Jolla, CA) (56). A receptor preparation tool was employed for protein structures preparation. The main steps involved were (i) energy minimization (using default force field), (ii) H-atoms and gastegier charges addition, (iii) Deletion of water molecules and native ligand (i.e. 2-oxo-1,2-dihydroquinoline for DNA gyrase and 1-(3-amino-2-methylbenzyl)-4-[2-(thiophen-2-yl)ethoxy]pyridin-2(1H)-one for FabI). In each case, the active pocket was identified around the co-crystallized ligandwithin 5 Å vicinity.

The synthesized samples as ligands (CNC-g-PVP and CNC-g-PVP doped CdS QDs) were built by modification of cellulose and PVP structure obtained from PubChem using ligedit tool of ICM. The top ten conformations were generated for monomer unit of each sample using the conformational analysis tool and finally performed optimization. The best-docked conformation was selected in each case for further analysis.

3. RESULTS AND DISCUSSION

3.1. XRD

The XRD spectrum for CdS, 1:0, and 1:0 doped CdS QDs with 2θ range (20°-70°), prepared by co-precipitation, is shown in Fig. 2(a). The CdS (QDs) diffraction peaks obtained at 24.92° (100), 26.69° (002), 28.31° (101), 43.96° (110), 48.08° (103) and 52.15° (112) revealed planes of hexagonal crystal structure confirmed with (JCPDS card # 01-080-0006) (57) and also confirming the the high purity of the prepared product as no unwanted peak was observed. . Peaks at 12°, 19.5°, 22.4°, 33.9° exhibited by CNC-g-PVP indexed as (101), (002) and (112)

planes (58). The average crystallite size was calculated by the Debye Scherrer formula from 9.05-7.05 nm. Interestingly, no significant shift was observed upon doping in the graph, while sharpness in peaks expressed successful incorporation of CNC-g-PVP into CdS. However, no characteristic peak of the dopant was observed in any doped samples due to adding a relatively lower quantity in the product.

3.2. Fourier-transform infrared spectroscopy (FTIR)

The FTIR technique was manifested to study the transmission spectrum of infrared radiations for vibrational characterization. The spectra have two regions; first from 4000 to 1500 cm^{-1} range represents the distinctive bands of functional groups as "important" or "functional group region", and second from 1500 to 400 cm^{-1} is described as the "fingerprint region" (59). Fig. 2(b) shows the transmission bands at 3317, 1630, 1350, 1006, 835, and 790 cm^{-1} to identify different functional groups. The transmission bands found around 3313 and 1630 cm^{-1} manifested to the O-H stretching vibrations and symmetric bending vibrations of H_2O molecules, respectively (60, 61). The band identifies the presence of thiourea in the sample at 1350 cm^{-1} assigned to C-N and at 1006 cm^{-1} shows C-O stretching of ethers (62, 63). The bands found at 795 and 835 cm^{-1} in the lower wavelength region are associated with Cd–S bond stretching modes (59, 64). The dopant bands at 1112 and 668 cm^{-1} manifested the cellulose C-O-C stretching vibrations and OH out-of-plane flexion (47, 65, 66).

3.3. Selected area electron diffraction (SAED) pattern

SAED examined concentric rings related with planes (002), (100), (101), and (103) of as-prepared and doped samples are well-matched with XRD results verifying the hexagonal structure of CdS while indexed planes (002), (101) and (112) associated to dopant Fig. 2(c-g).

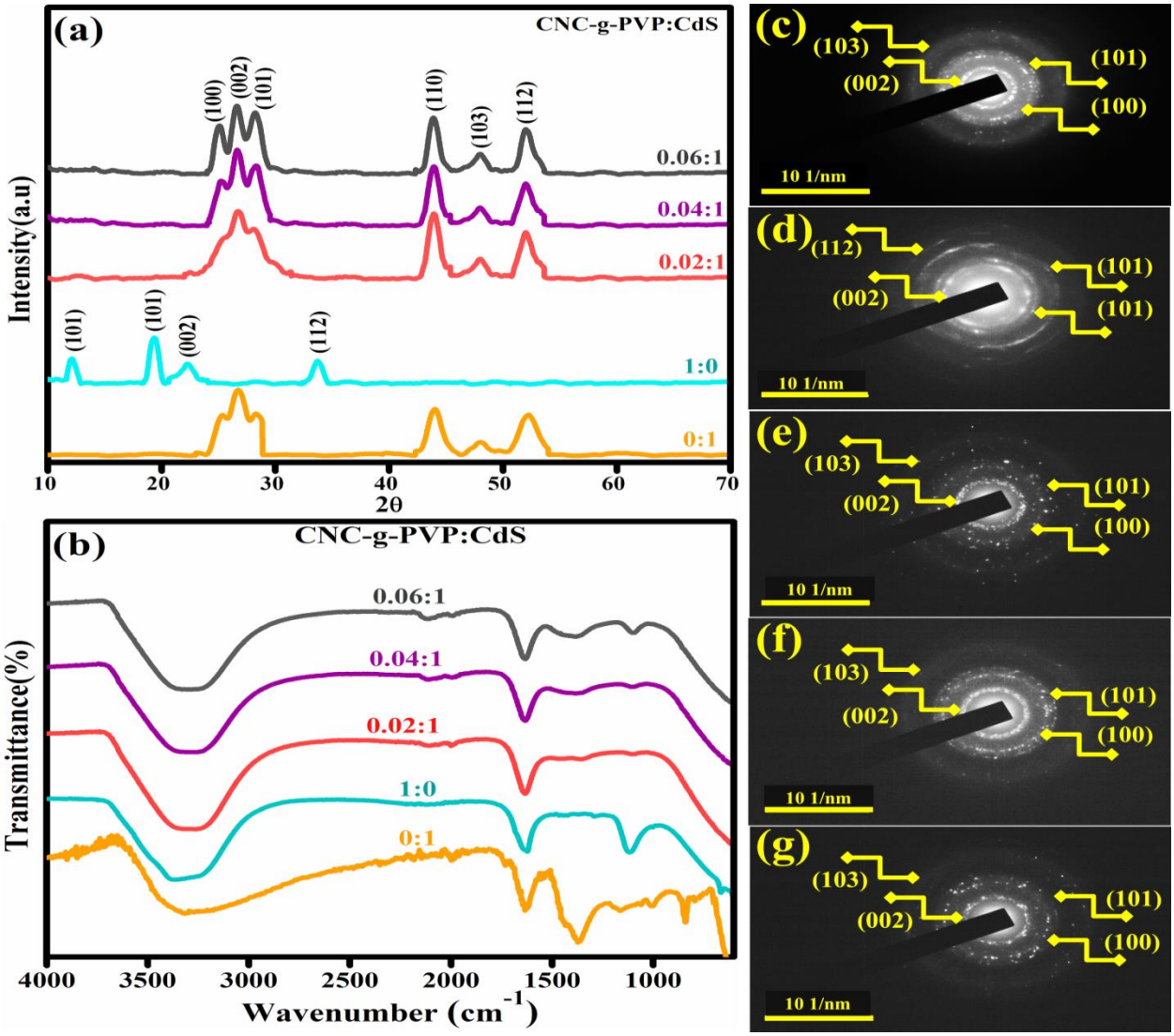

Fig.2. (a) XRD pattern, (b) FTIR spectra, (c–g) SAED pattern of CdS, CNC-g-PVP and CNC-g-PVP (2, 4, and 6%)/CdS

3.4.UV-Vis spectroscopy

To analyze the optical characteristic, synthesized samples (doped free CdS, dopant, and doped CdS) were examined using UV–vis absorption spectra, as illustrated in Fig. (3a). The n–π* transitions, including N lone pairs, have an absorption area ranging from 450 to 600 nm (67). The absorption band edge for CdS at 505 nm nominated the transition of electron (n–π*) amongst the 4d state of Cd and 3p state of S, respectively (42, 68). By Tauc's equation, the Eg values were calculated as 2.45, 3.2, 2.46, 2.49 and 2.51 eV for CdS, CNC-g-PVP and doped (2, 4, and 6%) CdS QDs, respectively. Upon doping, blue shift was observed in absorption spectra

that slightly increased Eg values manifested to quantum confinement effect (69, 70). The increase in band gap energy upon doping specifies a reduction in crystallite size.

3.5. Photoluminescence (PL) spectroscopy

The PL pattern of CdS, dopant, and doped CdS investigated from 500 to 650 nm to study recombination rate and change in electron transfer efficiency with an excitation wavelength of 350 nm, Fig. (3b). A single bright green emission band was found in PL spectra for the undoped sample at 550 nm (68). Spectra revealed the efficiency of charge transfer and electron-hole pair recombination (71). The CdS peak at 550 nm represented the lowest intensity, indicating low defects and high electron transfer efficiency. Doping enhanced the recombination rate of excitons and intensity, attributed to the reduction in electron transfer efficiency.

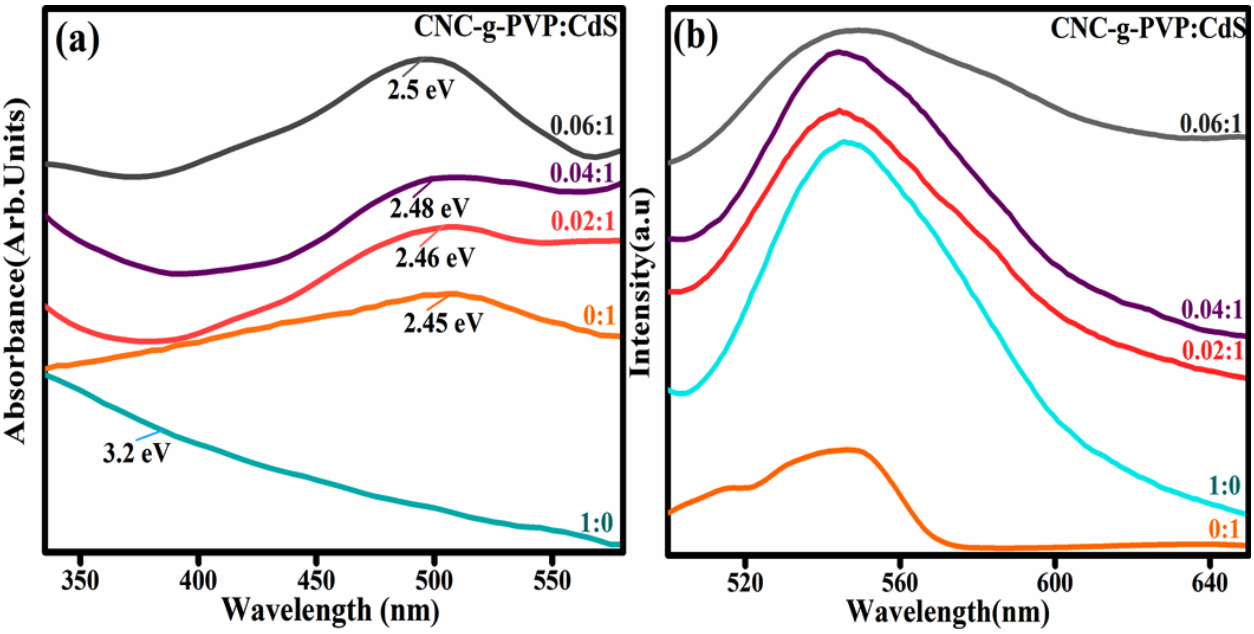

Fig. 3. (a) UV-Vis absorbance spectra, (b) PL spectra for pristine, dopant, and doped CdS QDs

3.6. Energy-dispersive X-ray spectroscopy (EDS) mapping study

EDS mapping of CNC-g-PAA:CdS with a weight ratio of 0.06:1 is shown in Fig. 4a. Identified six elements (C, Cd, Na, Au, S, O) were evenly distributed throughout specimen levels with different concentrations of elements via unique colors. Fig. 4(b-g) represented C, Cd, Na, Au, S, and O. EDS identified the elemental composition of prepared samples as shown in Fig. 4(a′-c′).

The pure sample affirmed by intense peaks of Cd and S (Fig. 4a′), while doped samples have a similar spectrum. In addition, peaks of carbon (C) and chlorine (Cl) were observed in samples attributed to precursor used during synthesis Fig. 4c′. The sodium (Na) peak for pure and doped samples was attributed to NaOH, added during synthesis of sample to maintain pH. Gold (Au) coating sprayed over the sample attributed to lessening charging impact, so Au peaks are shown in the spectra.

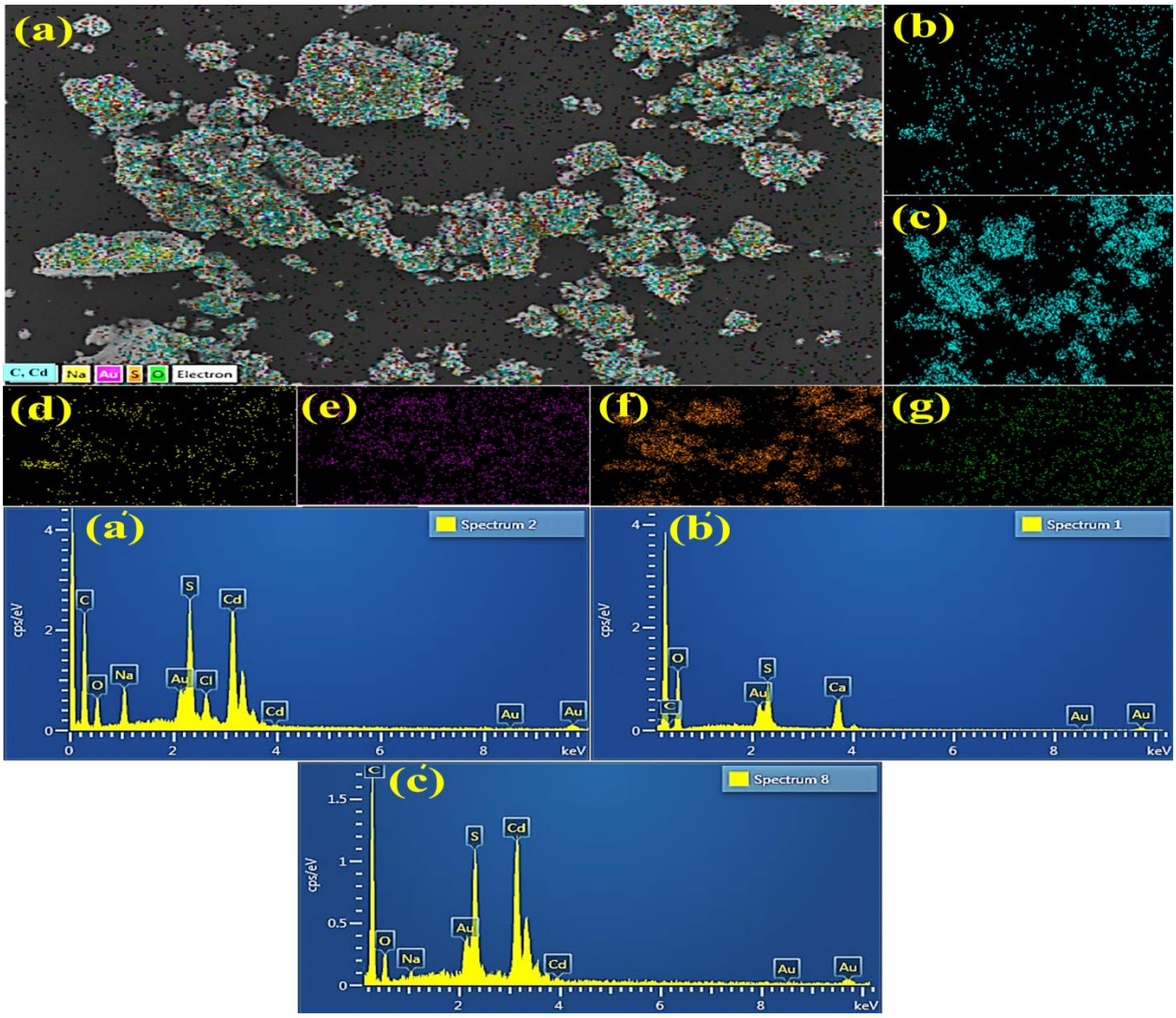

Fig.4. (a) EDS Mapping of doped sample prepared using weight ratio of CNC-g-PAA to Cds of 0.06:1 and identified elements shown in various colors. (b) Represent carbon (C) concentration and similarly (c-g) show Cd, Na, Au, S, and O, respectively. EDS patterns of synthesized samples with weight ratio of CNC-g-PAA to Cds: (a′) 0:1, (b′) 1:0, and (c′) 0.02:1.

3.7. Morphological analysis by field emission scanning electron microscopy (FESEM)

Fig. 5(a-d) illustrated the FESEM images for pristine, dopant, and doped samples. CdS revealed agglomerated non-uniform chunks with un-dissolved small-sized particles and dopant expressed acerose like structures having unequal sizes as shown in Fig. 5(a-b). 4% doped CdS having highly agglomerated large size acuminated chunks with un-soluble nano-sized particles and 6% doped CdS QDs unveiled breaking off large chunks with the increasing quantity of un-dissolved small particles, Fig. 5(c-d).

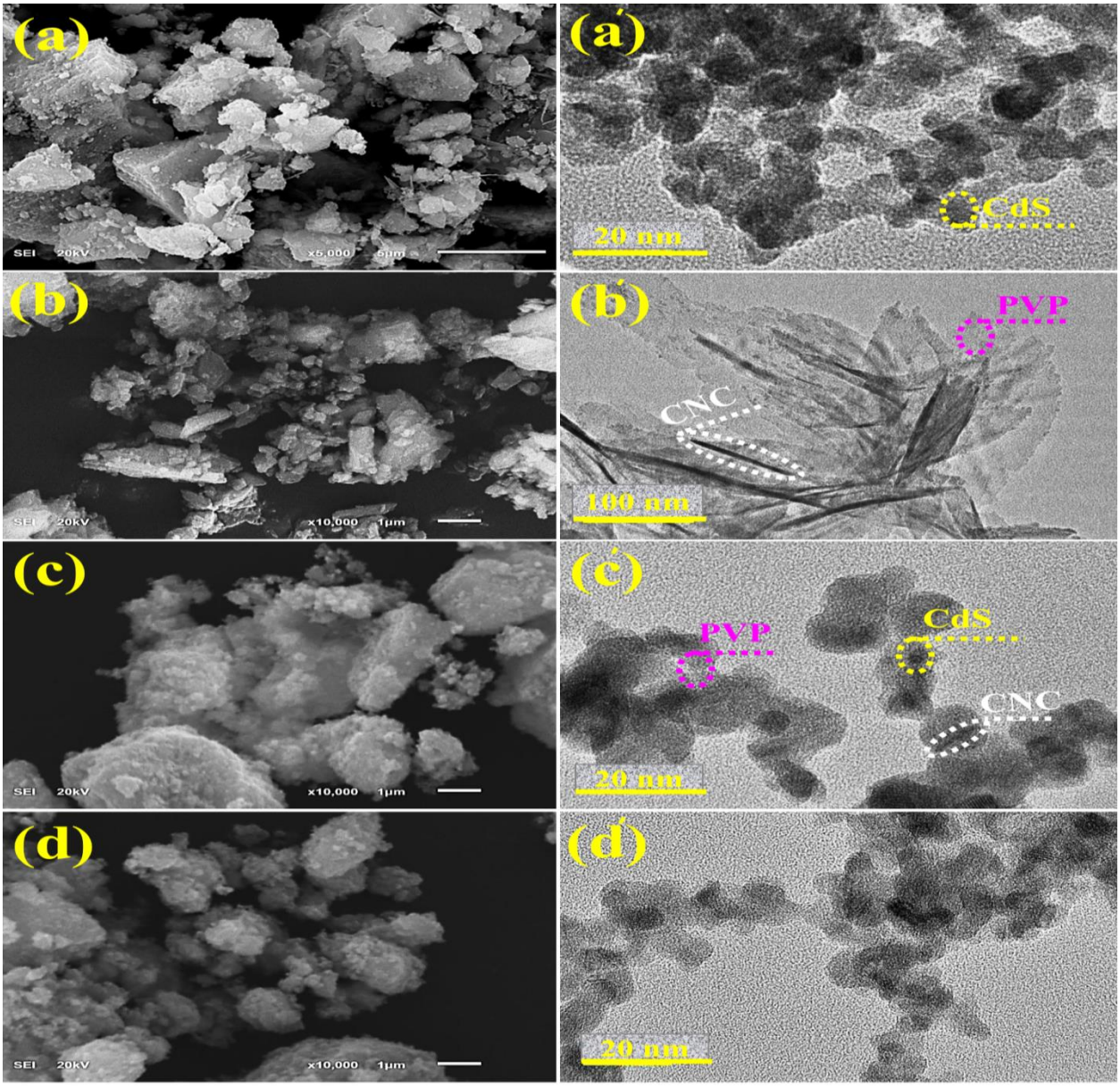

Fig.5. (a-d) FESEM and (a′-b′) TEM micrographs of prepared samples with weight ratio of grafted to doped CdS (QDs): (a, a′) 0:1, (b, b′) 1:0, (c, c′) 0.04:1 and (d, d′) 0.06:1.

3.1. High-resolution transmission electron microscopy (HR-TEM)

The morphological and structural analysis of samples was studied using TEM resolution up to 10 nm Fig. 5(a′-d′). The doped free CdS QDs sample (Fig. 5a′) reveals agglomerated particles having black-white phases with spherical morphology synthesized by the co-precipitation pathway. The dopant (CNC-g-PVP) has varied size rod-like morphology associated with CNC encapsulated in flower-like pattern PVP (Fig. 5(b′)). The addition of dopant (4%) in QDs

revealed a highly aggregated overlapped network of particles enfolded into a slightly thin dopant layer responsible for the nucleation process (Fig. 5c′). Furthermore, the higher concentration of dopant (6%) represented aggregation of particles highly stuck together attributed to PVP adhesive effect (72) and reduction in particle size. This change in particle size upon doping could be attributed to PVP concentration responsible to control the particle size of the product. The particle size, crystallite size, and Eg variations with different doping concentrations of CNC-g-PVP are illustrated in Table 1. When attraction forces dominate between the particles, agglomeration occurs. Particles adhere together loosely by overlapping QDs manifested to Brownian agglomeration to form a network of QDs (73, 74).

Table 1. Band gap, crystallite size, and particle size of pristine and doped CdS QDs

Samples	band gap energy (eV)	crystallite size (nm)	particle size (nm)
CdS QDs	2.45	9.05	9.28
Grafted (2%) doped CdS QDs	2.46	8.25	8.75
Grafted (4%) doped CdS QDs	2.49	7.43	7.85
Grafted (6%) doped CdS QDs	2.51	7.05	7.15

The d-spacing for CdS was 0.33 nm, which agrees with CdS theoretical d-spacing of the crystallographic plane (002), as shown in Fig. 6(a). The dopant d-spacing was 0.262 nm, and for doped samples (2, 4, and 6%) increased slightly (0.331-0.335 nm), as seen in Fig. 6(c-e), which matched with XRD results in Fig. 2(a).

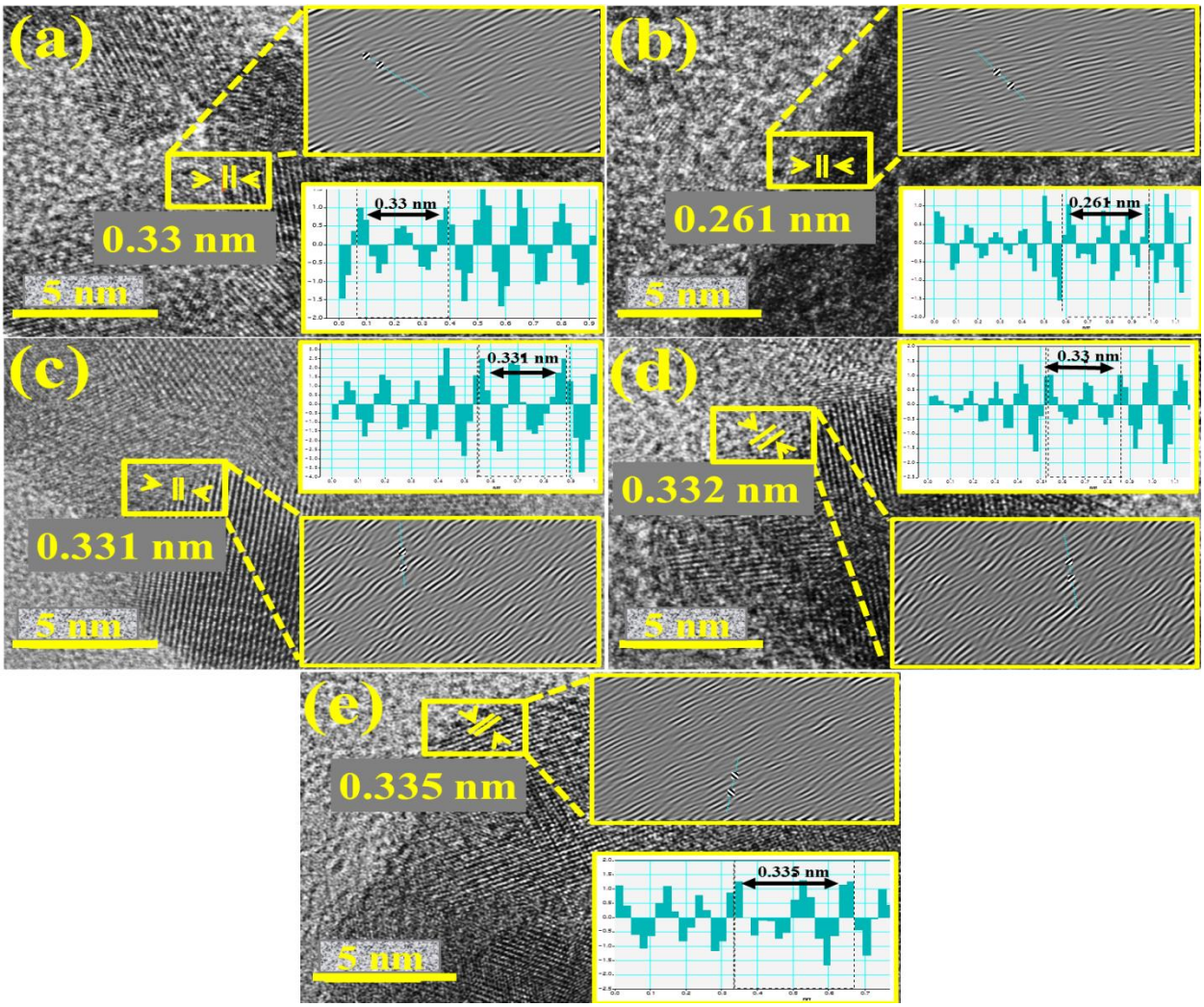

Fig. 6. (a-e) D-spacing of (0:1), (1:0) and (1:0) (2, 4, and 6%) doped (0:1) nanostructures.

3.2. Catalytic activity

The general mechanism for catalytic reduction having a reducing agent ($NaBH_4$) is superior to traditional approaches in terms of speed, simplicity, ease of operation, and recyclability. However, in the unavailability of a catalyst, this reaction is beneficial thermodynamically but unfavorable kinetically. At the start, the reactants (dye and $NaBH_4$) are adsorbed on catalyst surface, and $NaBH_4$ detaches into ions where BH_4^- operates as a donor and H^+ electron-accepting species. By releasing H_2 into the reaction mixture, $NaBH_4$ speeds up the process and reduces the time to activate the QDs by rebuilding their surface. For removal of H_2, the reaction is (75)

$$NaBH_4 + 2H_2O \longrightarrow NaBO_2 + 8H_2$$

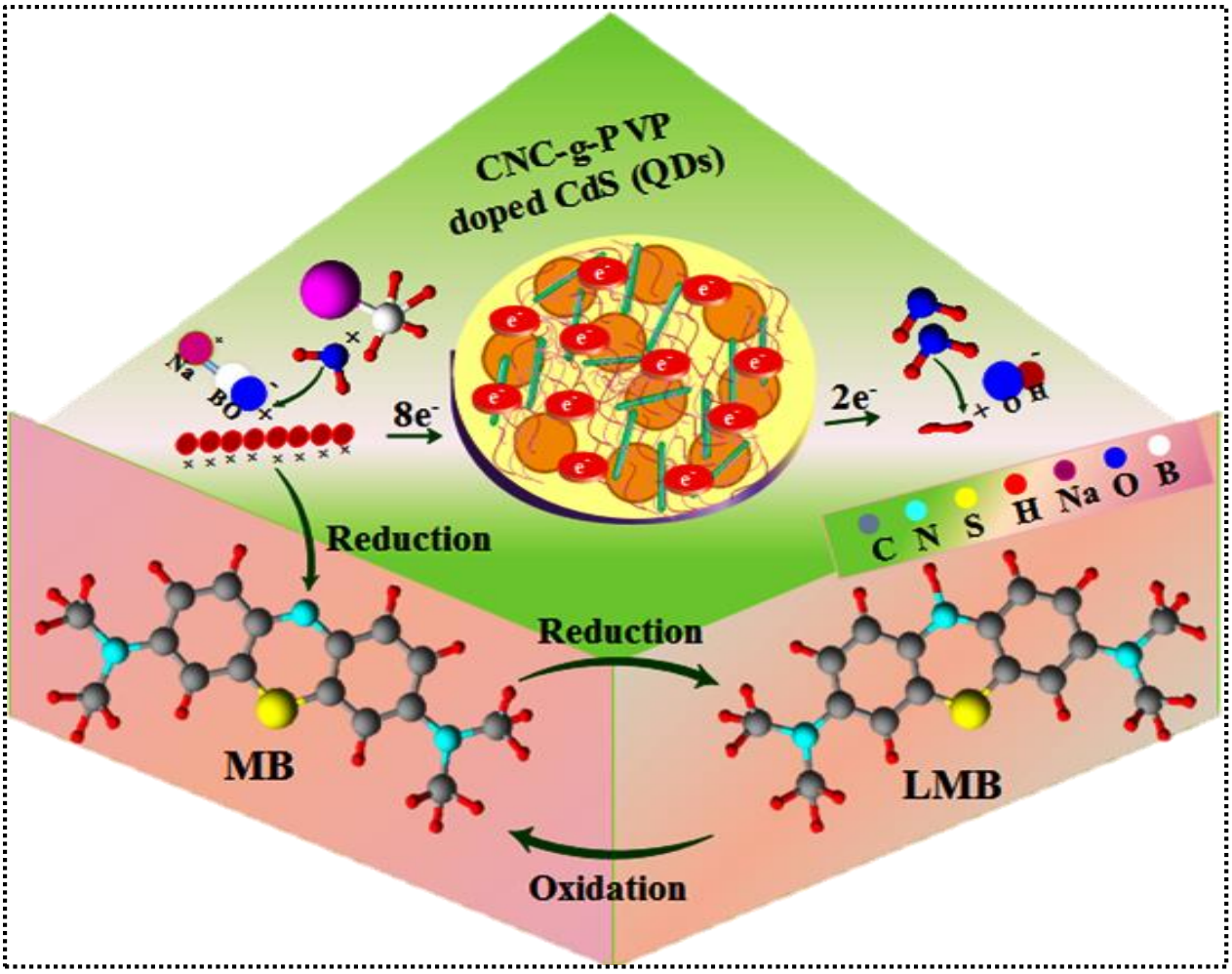

Fig. 7. CNC-g-PVP doped CdS QDs catalysis mechanism

During catalysis, the redox reaction involves the donation of e^- by $NaBH_4$ and electron accepted by MB (an oxidizing agent) resulting in synthetic dye breakdown. MB was also tested in the occurrence of a reducing agent, however, the reaction was quite sluggish in the absence of a nanocatalyst. The introduction of catalyst (as-prepared, grafted and doped samples) in an oxidation-reduction reaction enhanced the reaction rate by decreasing the activation energy necessary to start and progress the reaction quickly. The presence of a reducing agent and nanocatalyst increased degradation efficiency, indicating that $NaBH_4$ does not act as a catalyst (76). The cationic dye MB gains electrons and H atoms from BH_4^-, resulting in π conjugation, which breaks the double bond amongst the dye's N and aromatic rings. The MB molecule's doubly bonded N atom attaches H atom by breaking the double bond, whereas the positively charged N atom accepts an electron, resulting in π conjugation. The catalyst functions as electron

relay among reactant species and allows transfer of e^- from donor BH_4^- to the MB accepter, and as a result MB reduced to LMB, (Fig. 7). During CA, the amount of catalyst used in the reaction is an important factor as the extent of dye degradation increases with the increases in catalyst amount (75, 77).

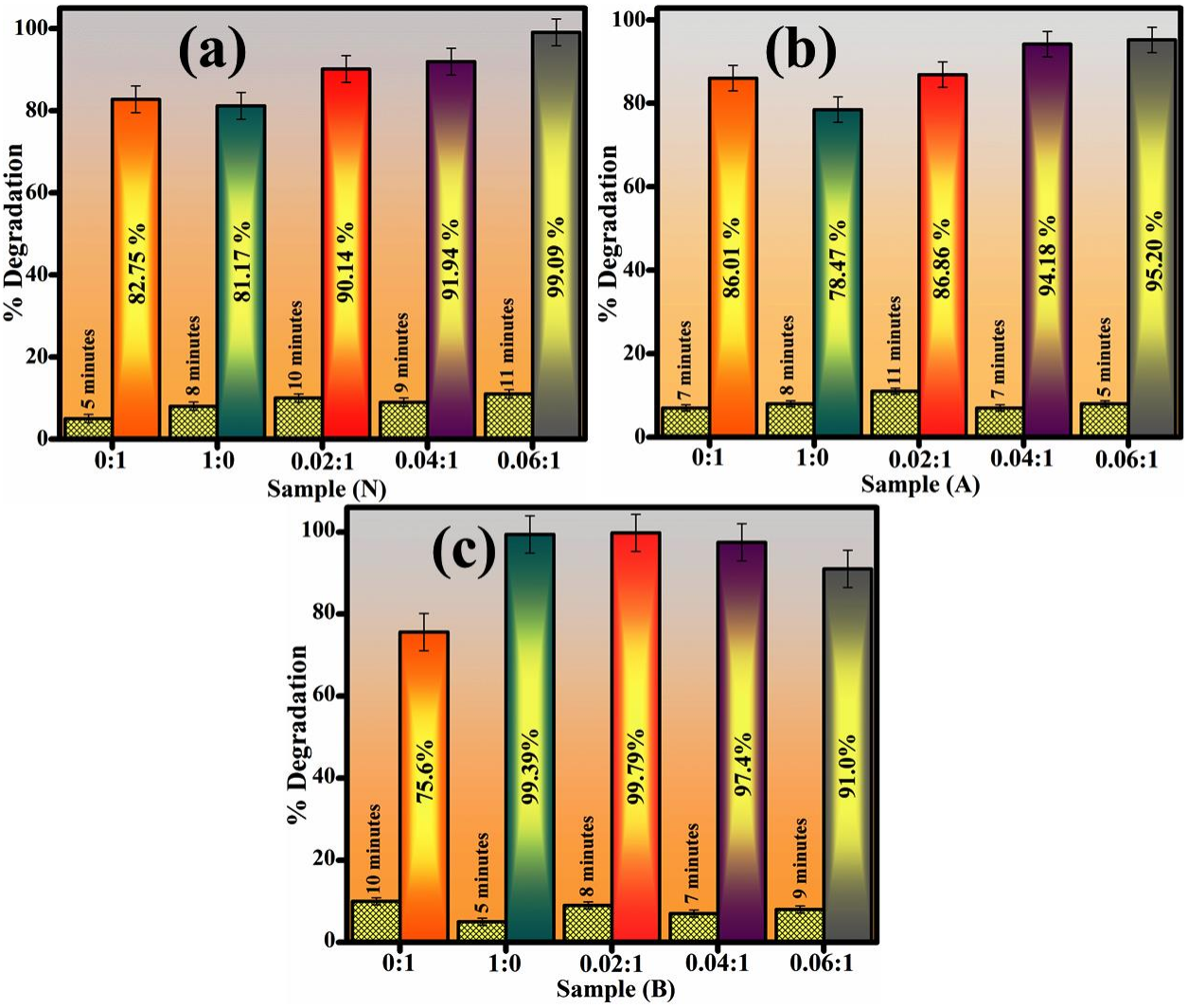

Fig. 8. Catalytic process of as-prepared, grafted and doped (2, 4, and 6%) QDs in (a) neutral, (b) acidic and (c) basic medium

A UV-vis spectrophotometer was employed to examine the impact of prepared, grafted, and doped QDs on MB degradation during catalysis. Undoped, grafted, and doped (2, 4, and 6%) CdS QDs explored degradation of 82.14, 81.19, 90.14, 91.14, and 99.09% at time interval of 5, 8, 10, 9 and 11 minutes in neutral; 86, 78.47, 86.86, 94.18, and 95.20% at time 7, 8, 11, 7 and 5

minutes in acidic; and 75.6, 99.39, 99.79, 97.4, and 91% at 10, 5, 8, 7 and 9 minutes in basic medium, respectively, as indicated in Fig. 8(a-c). The CA is influenced by pH of the medium, surface area, crystallinity, and morphology of QDs. The promising increase in degradation of MB was examined for grafted and (2%) doped CdS in basic medium, and higher doping concentrations (4 and 6%) resulted in lower dye degradation performance describing the optimum doping concentration in CdS for the greatest catalytic performance was 2%. The remarkable results in the basic medium for catalytic degradation are also attributed to MB cationic behavior, so MB adsorption on the catalyst surface increased (78). In acidic medium, maximum degradation for 6% doped CdS sample is manifested to higher production of H^+ ions absorbed onto the QDs surface. As a result, the increase in catalytic effectiveness for all mediums reported in this study is attributable to morphology change of QDs, which served to raise the surface area for reaction, and surface-to-volume ratio manifested in particle size reduction (79).

3.10. Antibacterial activity

The antibacterial activity of pristine, grafted, and doped CdS composites, as opposed to *S. aureus* and *E. coli*, isolated from caprine and bovine mastitic milk was defined by well diffusion technique as graphically demonstrated in Fig. 9a-d and Table 2. Apart from CdS, grafted samples showed zero results in antibacterial activity, which well matched with literature (50). The synergistic effect of grafted-doped CdS improved bactericidal activity as significant opposition was observed in grafted-doped CdS (4% and 6%) against *E. coli* and *S. aureus.* Inhibition diameters for pristine, dopant, and doped samples were observed between (0±0.0 – 3.60±0.4 mm) and (0±0.0 - 4.55±0.4 mm) at minimal, and similarly, (1.05±0.7 – 4.05±0.3 mm) and (1.15±0.8 - 5.25±0.5 mm) at maximal dosages against G -ve and G +ve strains, respectively (Fig. 9a-b). For *E. coli* at lower and upper concentrations, the % age efficiency of pure and doped CdS QDs was enhanced as (0–84.7%) and (14–95.5%), while the % age efficiency of as-prepared and doped samples for *S. aureus* at both concentrations was increased as (0–72.8%) and (17.6–84%), correspondingly (Fig.9c-d).

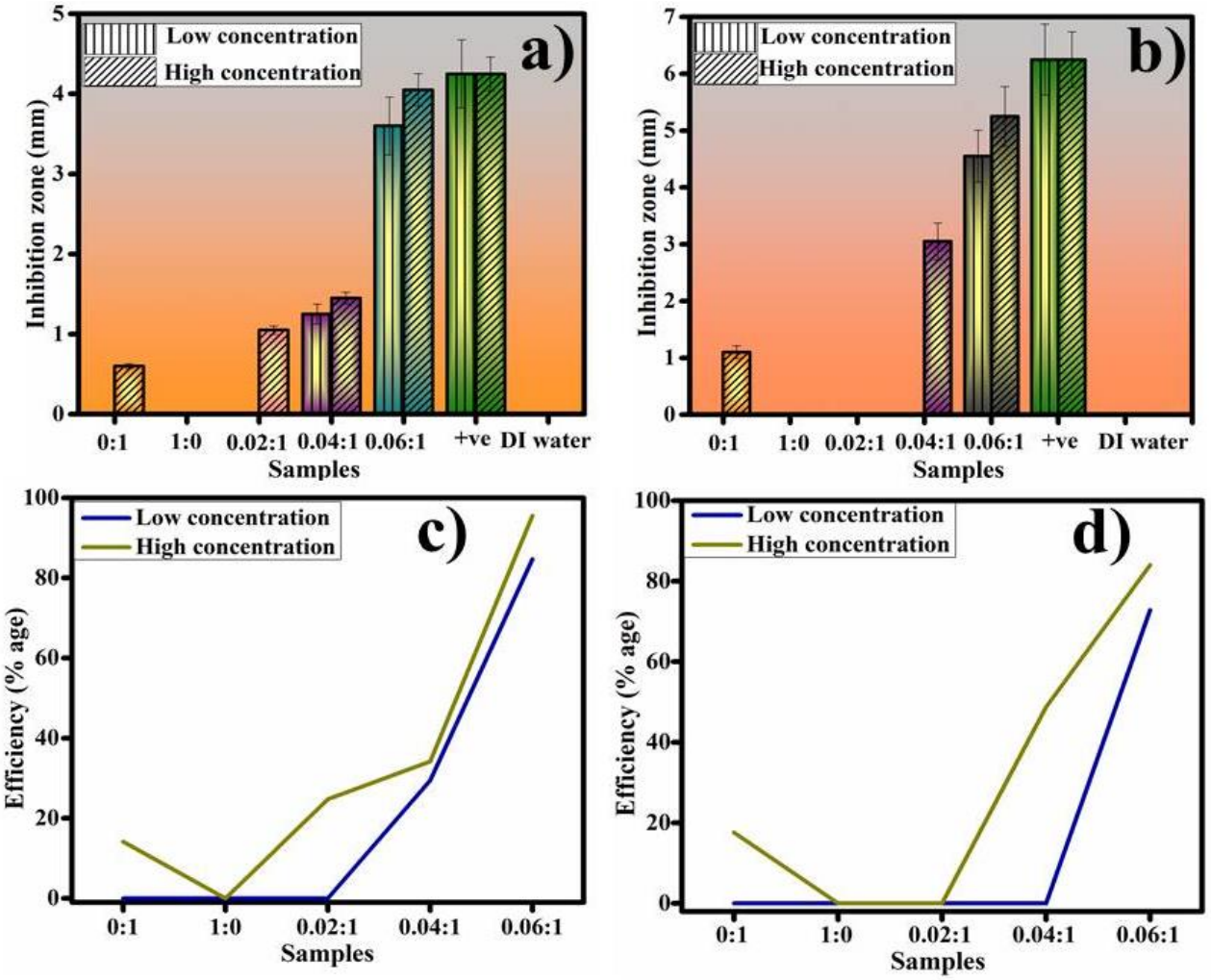

Fig. 9. In vitro bactericidal action of pure, dopant, and doped CdS QDs for *E. coli* (a) and *S. aureus* (b), and correspondingly efficiency %age comparison of CdS, grafted, and doped QDs for G–ve (c) and G+ve (d) bacteria.

Table2. Antibacterial activity of pristine, dopant and (2, 4, and 6%) doped CdS QDs.

Samples	Inhibition zone (mm) for *S. aureus*		Inhibition zone (mm) for *E. coli*	
	500 µg/50 µL	1000 µg/50 µL	500 µg/50 µL	1000 µg/50 µL
CdS	0±0.0	1.15±0.8	0±0.0	0.6±0.4
CNC-g-PVP	0±0.0	0±0.0	0±0.0	0±0.0
2%	0±0.0	0±0.0	0±0.0	1.05±0.7
4%	0±0.0	3.05±0.2	1.25±0.1	1.45±0.1

6% Ciprofloxacin	4.55±0.4	5.25±0.5	3.60±0.4	4.05±0.3
	6.25±0.0	6.25±0.0	4.25±0.0	4.25±0.0
DI water	0±0.0	0±0.0	0±0.0	0±0.0

CdS has a reduced antibacterial action due to cadmium's actions being restricted to a single channel of inhibition in which cadmium is able to enter cell membranes and occupy replicative potential, culminating in a bactericidal response (80). Moreover, grafted-doped CdS composites displayed a significant increase in % age efficiency against G-ve strain compared to G+ve. Because G+ve bacteria have thick peptidoglycan and strong chitinoid cell wall that may offer more resistance to QDs, while G-ve cell wall contains thin and multilayered lipid components that show less resistance towards the entering of QDs (2, 81, 82).

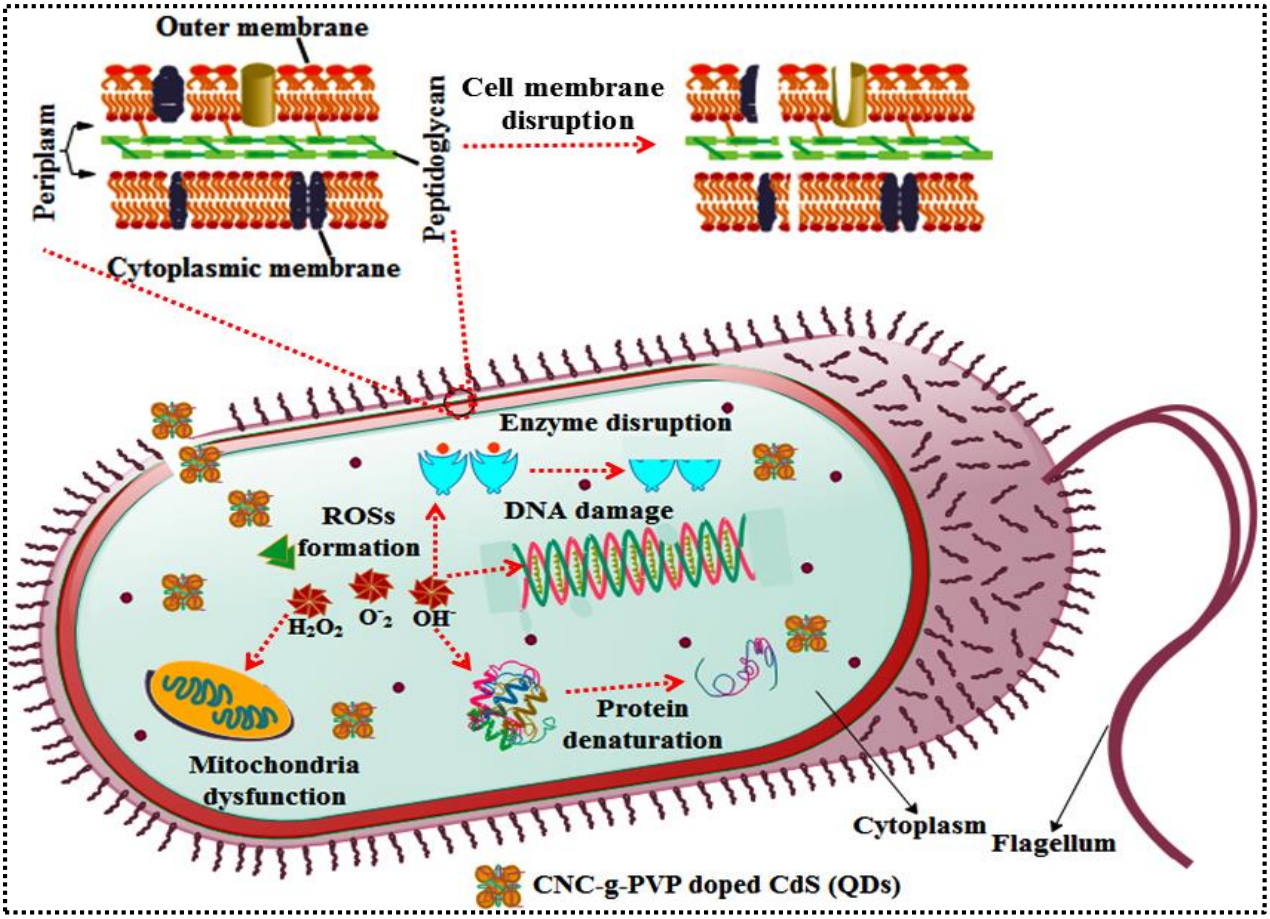

Fig. 10. Bactericidal behavior of CNC-g-PVP-doped CdS QDs

Further, QDs can suppress microbiological organisms primarily through three molecular mechanisms: the destruction of cell walls/cell membranes, reactive oxygen species (ROS) formation, and binding with genetic material (DNA/RNA) to stop cell replication. QDs are functionalized with polymers that may produce more ROS and strengthen their adhesion to bacterial components (83). Microbicidal efficacy of QDs also depends on their diameter and concentration, as size of QDs has an inverse proportion with microbicidal efficacy. The smaller diameter QDs efficiently produce ROS that insert bacterial cell membrane destruction, leading to bacterial burst via expulsion of cytoplasmic organelles. It is believed that the electrostatic interference between anionic bacterial membrane components and cationic Cd^{+2} ions is accountable for pathogenic bacteria mortality (84) as illustrated in Fig. 10.

3.3.Molecular docking study

Bacterial survival and growth depends on biosynthesis of various metabolites vital for functioning of various cell organelles. Biosynthetic pathways like cell wall synthesis, fatty acid synthesis, folic acid synthesis, nucleic acid synthesis etc. are essential for bacterial growth. Enzymes belonging to these biosynthetic pathways have been considered as attractive targets for antibiotic discovery as their inhibition decrease cell growth and ultimately cause death of bacteria (85).

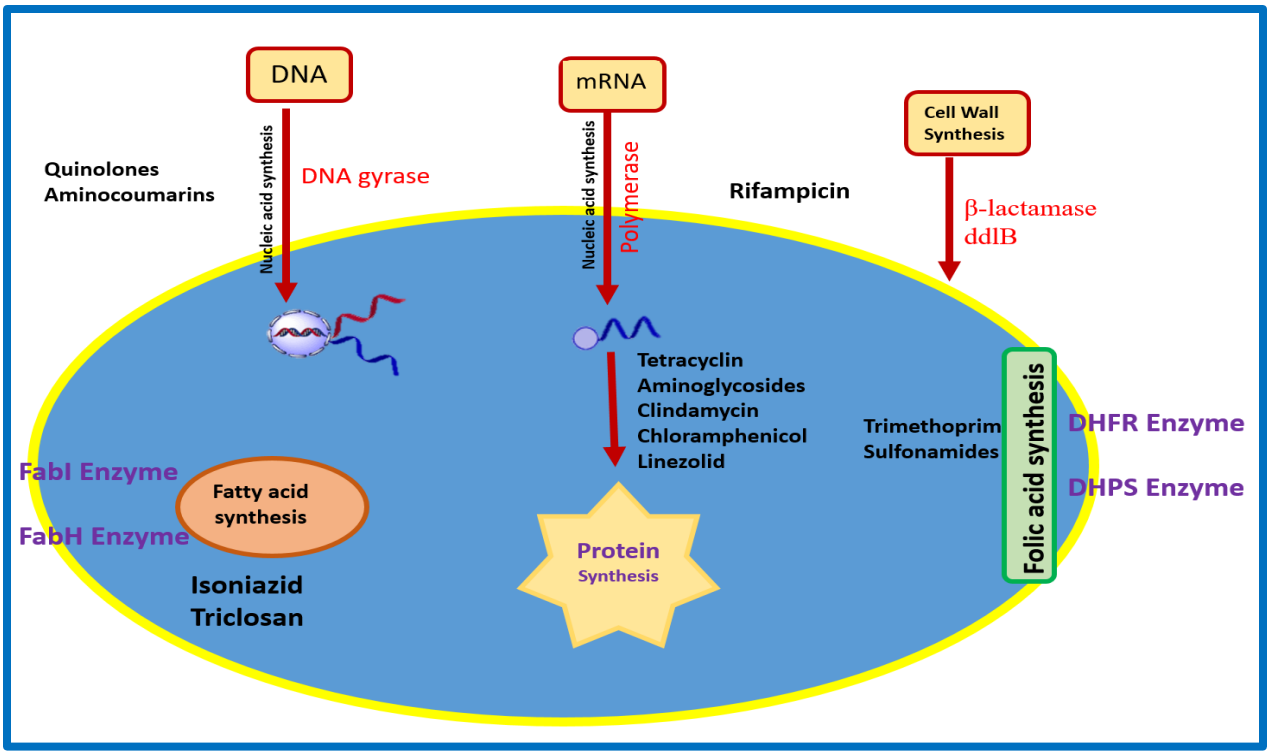

Fig. 11: Biosynthetic pathways, target enzymes and previously reported antibiotics

The important enzyme targets and drugs effective against them have been shown in Fig. 11. *In silico* studies facilitate in depth analysis of binding and interaction capacity of drug leads against given enzyme target. We performed molecular docking studies of our nanocomposites to evaluate their entrance inside active pocket of DNA gyrase (Nucleic acid synthesis) and FabI enzyme (Fatty acid synthesis) and to analyze binding interactions within docked complexes. Although the antimicrobial and bactericidal potential of PVP conjugated nanocomposites has been previously reported, however, the exact mechanism behind these biological activities is not clear (53). In recent decades, *in silico* molecular docking studies enabled scientists to rationalize mysteries behind various biological phenomena. The DNA gyrase belonging to the nucleic acid biosynthetic pathway and FabI of the fatty acid biosynthetic pathway is well-known and attractive targets for antibiotic discovery (86, 87). The binding interaction patterns for monomer units of CNC-g-PVP and CNC-g-PVP doped CdS QDs inside the active pocket of DNA gyrase$_{E.\ coli}$ and FabI$_{S.\ aureus}$ is depicted in Fig. 12 and 13, respectively.

In silico predictions were in good agreement with bactericidal activities shown by CNC-g-PVP and CNC-g-PVP doped CdS QDs. Although no considerable antibacterial activity was observed

for CNC-g-PVP while CNC-g-PVP doped CdS QDs showed good bactericidal potential against both *E. coli* and *S. aureus*, where similar trends were observed for *in silico* predictions. As shown in Fig. 12, for DNA gyrase$_{E.\ coli}$, the CNC-g-PVP revealed H-bonding with Thr165 (2.8 Å) and Asp73 (3.3 Å), having binding score of -4.528 kcal/mol while CNC-g-PVP doped CdS QDs showed four H-bonds with Thr165 (2.6 Å), Asp73 (3.1 Å & 3.3 Å), and Glu50 (2.8 Å) alongside hydrophobic interaction with Asn46 and Ile78 having binding score -8.773 kcal/mol.

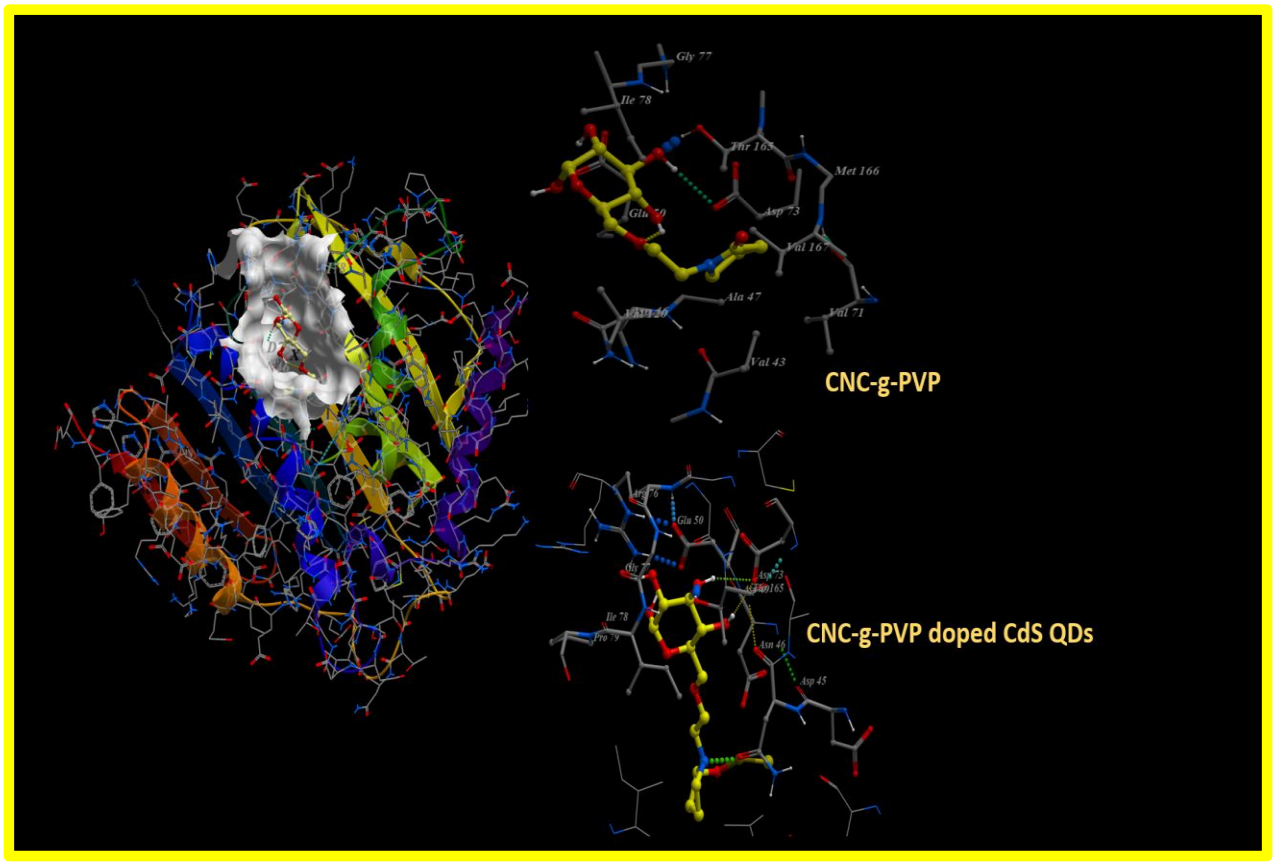

Fig. 12: Binding interaction pattern of CNC-g-PVP and CNC-g-PVP doped CdS QDs inside active pocket of DNA gyrase$_{E.\ coli}$

Similarly, for FabI$_{S.\ aureus}$, the best docked conformation observed for CNC-g-PVP revealed H-bonding interactions with Thr195 (2.9 Å) and Gly191 (3.2 Å) with an overall binding score of -3.928 kcal/mol while CNC-g-PVP doped CdS QDs showed a considerably high binding score of -9.756 kcal/mol having H-bonds with Tyr157 (2.9 Å), Ile193 (2.7 Å), Thr195 (2.8 Å) alongside hydrophobic interactions with Phe96, Ala198, and Val201, as depicted in Fig. 13.

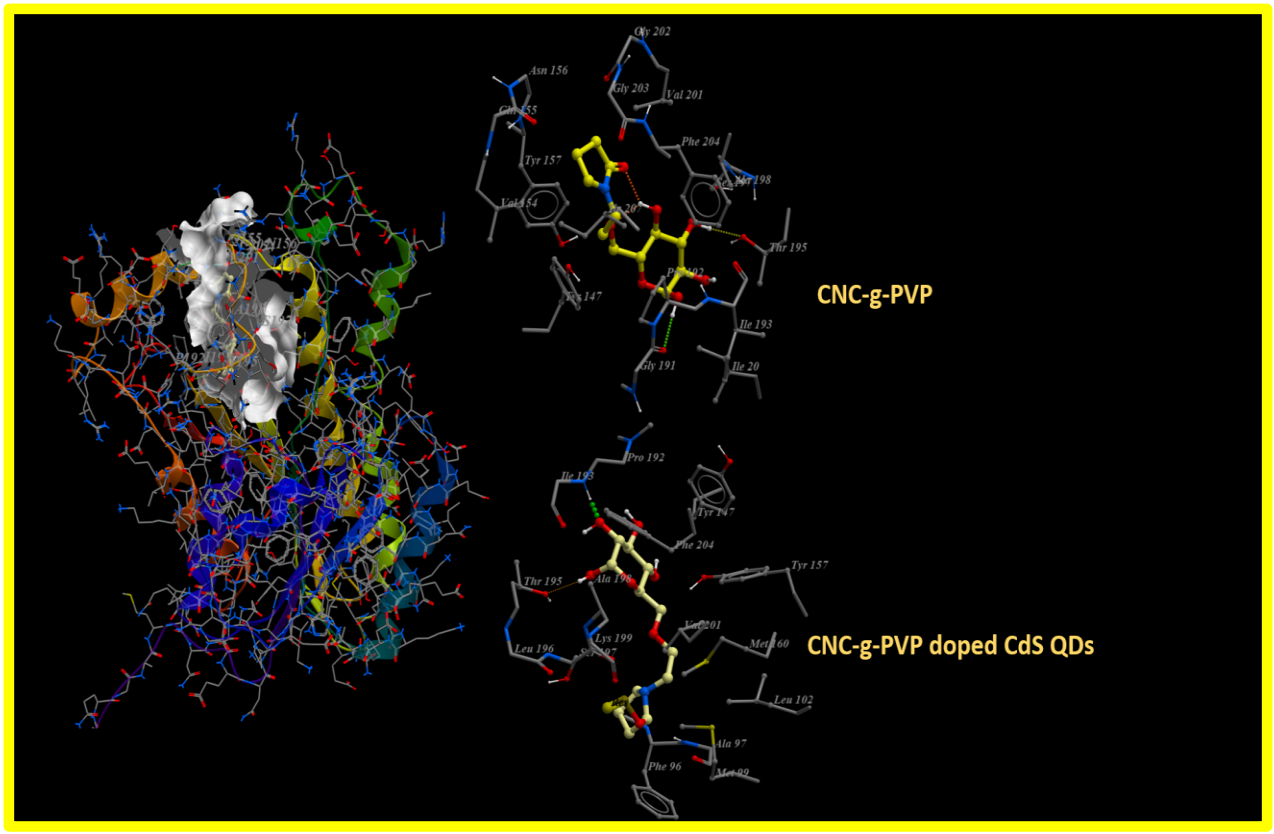

Fig. 13: Binding interaction pattern of CNC-g-PVP and CNC-g-PVP doped CdS QDs inside active pocket of FabI*S. aureus*

4. CONCLUSION

In this study, synthesized samples (CdS, CNC-g-PVP, and CNC-g-PVP doped CdS (QDs) with varying concentrations (2, 4 and 6%) of CNC-g-PVP) were effectively prepared using a low-cost co-precipitation technique. Several characterizations were employed to examine the synthesized QDs. XRD spectra affirmed the presence of hexagonal phase. The presence of all ingredient functional groups in prepared QDs was confirmed through FTIR, which is further evaluated by EDS spectra to confirm the presence of elemental composition of pristine and doped samples. UV-vis spectroscopy exposed that the absorption peaks for doped samples accompanied a blue shift compared to undoped samples attributed to the quantum confinement effect. The TEM images revealed the spherical morphology of CdS QDs, and upon doping, particle size decreased from 9.28 nm to 7.15 nm. Doped QDs indicated higher catalytic activity up to 99.76%. Moreover, the doped CdS QDs have expressed significant bactericidal effects against pathogenic etiologies such as *S. aureus* and *E. coli*. In silico predictions were in good agreement along in

vitro bactericidal activities and suggested the inhibitory role of CNC-g-PVP doped CdS (QDs) against DNA gyrase and FabI. In summary, CdS QDs with natural and synthetic polymers could be environmentally friendly, economical, and effective against bacteria and industrial dye degrader. This research indicates that by using doped QDs as antimicrobials placebos, the potential pathogenic etiologies could be considerably addressed.

Acknowledgement: Authors are thankful to HEC Pakistan through Project NRPU-20-17615

Conflict of Interest: No conflict of interest

REFERENCES

1. Wang Z, Wu A, Colombi Ciacchi L, Wei G. Recent advances in nanoporous membranes for water purification. Nanomaterials. 2018;8(2):65.
2. Shaheen S, Iqbal A, Ikram M, Ul-Ain K, Naz S, Ul-Hamid A, et al. Effective Disposal of Methylene Blue and Bactericidal Benefits of Using GO-Doped MnO2 Nanorods Synthesized through One-Pot Synthesis. ACS omega. 2021;6(38):24866-78.
3. Liu L, Zhang B, Zhang Y, He Y, Huang L, Tan S, et al. Simultaneous removal of cationic and anionic dyes from environmental water using montmorillonite-pillared graphene oxide. Journal of Chemical & Engineering Data. 2015;60(5):1270-8.
4. Shaban M, Ashraf AM, Abukhadra MR. TiO2 nanoribbons/carbon nanotubes composite with enhanced photocatalytic activity; fabrication, characterization, and application. Scientific Reports. 2018;8(1):1-17.
5. Rafiq A, Imran M, Aqeel M, Naz M, Ikram M, Ali S. Study of transition metal ion doped CdS nanoparticles for removal of dye from textile wastewater. Journal of Inorganic and Organometallic Polymers and Materials. 2020;30(6):1915-23.
6. Albukhari SM, Ismail M, Akhtar K, Danish EY. Catalytic reduction of nitrophenols and dyes using silver nanoparticles@ cellulose polymer paper for the resolution of waste water treatment challenges. Colloids and Surfaces A: Physicochemical and Engineering Aspects. 2019;577:548-61.
7. Aziz KHH, Miessner H, Mueller S, Mahyar A, Kalass D, Moeller D, et al. Comparative study on 2, 4-dichlorophenoxyacetic acid and 2, 4-dichlorophenol removal from aqueous solutions via ozonation, photocatalysis and non-thermal plasma using a planar falling film reactor. Journal of hazardous materials. 2018;343:107-15.
8. Fu W, Zhang W. Microwave-enhanced membrane filtration for water treatment. Journal of Membrane Science. 2018;568:97-104.
9. Salimi F, Emami SS, Karami C. Removal of methylene blue from water solution by modified nano-boehmite with Bismuth. Inorganic and Nano-Metal Chemistry. 2018;48(1):31-40.
10. Nasrollahzadeh M, Issaabadi Z, Sajadi SM. Green synthesis of a Cu/MgO nanocomposite by Cassytha filiformis L. extract and investigation of its catalytic activity in the reduction of methylene blue, congo red and nitro compounds in aqueous media. RSC advances. 2018;8(7):3723-35.
11. Nasrollahzadeh M, Sajjadi M, Sajadi SM. Biosynthesis of copper nanoparticles supported on manganese dioxide nanoparticles using Centella asiatica L. leaf extract for the efficient catalytic reduction of organic dyes and nitroarenes. Chinese Journal of Catalysis. 2018;39(1):109-17.

12. Hassan J, Ikram M, Ul-Hamid A, Imran M, Aqeel M, Ali S. Application of chemically exfoliated boron nitride nanosheets doped with co to remove organic pollutants rapidly from textile water. Nanoscale research letters. 2020;15(1):1-13.
13. Dou R, Cheng H, Ma J, Komarneni S. Manganese doped magnetic cobalt ferrite nanoparticles for dye degradation via a novel heterogeneous chemical catalysis. Materials Chemistry and Physics. 2020;240:122181.
14. K. Alharbi N, Alsaloom AN. Characterization of Lactic Bacteria Isolated from Raw Milk and Their Antibacterial Activity against Bacteria as the Cause of Clinical Bovine Mastitis. Journal of Food Quality. 2021;2021:6466645.
15. Ryman VE, Packiriswamy N, Sordillo LM. Role of endothelial cells in bovine mammary gland health and disease. Animal health research reviews. 2015;16(2):135-49.
16. Malik TA, Mohini M, Mir S, Ganaie B, Singh D, Varun T, et al. Somatic cells in relation to udder health and milk quality-a review. Journal of Animal Health and Production. 2018;6(1):18-26.
17. Jensen K, Günther J, Talbot R, Petzl W, Zerbe H, Schuberth H-J, et al. Escherichia coli-and Staphylococcus aureus-induced mastitis differentially modulate transcriptional responses in neighbouring uninfected bovine mammary gland quarters. BMC genomics. 2013;14(1):1-19.
18. Chandrasekaran S, Yao L, Deng L, Bowen C, Zhang Y, Chen S, et al. Recent advances in metal sulfides: from controlled fabrication to electrocatalytic, photocatalytic and photoelectrochemical water splitting and beyond. Chemical Society Reviews. 2019;48(15):4178-280.
19. Sarker JC, Hogarth G. Dithiocarbamate complexes as single source precursors to nanoscale binary, ternary and quaternary metal sulfides. Chemical Reviews. 2021;121(10):6057-123.
20. Tamilselvan M. Metal Sulphide Based Semiconductors for Solar Photon Energy Harvesting 2021.
21. Khalil AT, Khan MD, Razzaque S, Afridi S, Ullah I, Iqbal J, et al. Single precursor-based synthesis of transition metal sulfide nanoparticles and evaluation of their antimicrobial, antioxidant and cytotoxic potentials. Applied Nanoscience. 2021;11(9):2489-502.
22. Zhang X, Zhao Y, Zhang C, Wu C, Li X, Jin M, et al. Cobalt sulfide embedded carbon nanofibers as a self-supporting template to improve lithium ion battery performances. Electrochimica Acta. 2021;366:137351.
23. Indhumathi C, Manikandan A. Synthesis, morphological, magneto-optical and photocatalytic properties of MnZn1− xS nano-catalysts. Malaya Journal of Matematik (MJM). 2020(2, 2020):718-20.
24. Zhang K, Lv S, Lin Z, Tang D. CdS: Mn quantum dot-functionalized g-C3N4 nanohybrids as signal-generation tags for photoelectrochemical immunoassay of prostate specific antigen coupling DNAzyme concatamer with enzymatic biocatalytic precipitation. Biosensors and Bioelectronics. 2017;95:34-40.
25. Cai G, Yu Z, Ren R, Tang D. Exciton–plasmon interaction between AuNPs/graphene nanohybrids and CdS quantum dots/TiO2 for photoelectrochemical aptasensing of prostate-specific antigen. ACS sensors. 2018;3(3):632-9.
26. Zhang K, Guo L. Metal sulphide semiconductors for photocatalytic hydrogen production. Catalysis Science & Technology. 2013;3(7):1672-90.
27. Junaid M, Imran M, Ikram M, Naz M, Aqeel M, Afzal H, et al. The study of Fe-doped CdS nanoparticle-assisted photocatalytic degradation of organic dye in wastewater. Applied Nanoscience. 2019;9(8):1593-602.
28. Kadam SR, Gosavi SW, Kale BB, Suzuki N, Terashima C, Fujishima A. Unique CdS@ MoS2 core shell heterostructure for efficient hydrogen generation under natural sunlight. Scientific reports. 2019;9(1):1-10.
29. Ikhmayies SJ. Fine-Structured Red-Band Tail Photoluminescence (PL) Spectra of Nanocrystalline CdS: In Thin Films. JOM. 2021;73(5):1261-70.

30. Ibrahim I, Lim HN, Zawawi RM, Tajudin AA, Ng YH, Guo H, et al. A review on visible-light induced photoelectrochemical sensors based on CdS nanoparticles. Journal of Materials Chemistry B. 2018;6(28):4551-68.
31. Khan ZR, Shkir M, Alshammari AS, Ganesh V, AlFaify S, Gandouzi M. Structural, linear and third order nonlinear optical properties of sol-gel grown Ag-CdS nanocrystalline thin films. Journal of Electronic Materials. 2019;48(2):1122-32.
32. Luo Z, Zhang L, Zeng R, Su L, Tang D. Near-infrared light-excited core–core–shell UCNP@ Au@ CdS upconversion nanospheres for ultrasensitive photoelectrochemical enzyme immunoassay. Analytical chemistry. 2018;90(15):9568-75.
33. Zeng R, Luo Z, Su L, Zhang L, Tang D, Niessner R, et al. Palindromic molecular beacon based Z-scheme BiOCl-Au-CdS photoelectrochemical biodetection. Analytical chemistry. 2019;91(3):2447-54.
34. Bosio A, Rosa G, Romeo N. Past, present and future of the thin film CdTe/CdS solar cells. Solar Energy. 2018;175:31-43.
35. Sharma VK, Filip J, Zboril R, Varma RS. Natural inorganic nanoparticles–formation, fate, and toxicity in the environment. Chemical Society Reviews. 2015;44(23):8410-23.
36. AL-Jawad SM, Imran NJ, Aboud KH. Synthesis and characterization of Mn: CdS nanoflower thin films prepared by hydrothermal method for photocatalytic activity. Journal of Sol-Gel Science and Technology. 2021;100(3):423-39.
37. Yaseen M, Ambreen H, Zia M, Javed H, Mahmood A, Murtaza A. Study of half metallic ferromagnetism and optical properties of Mn-doped CdS. Journal of Superconductivity and Novel Magnetism. 2021;34(1):135-41.
38. Shaikh S, Shkir M, Masumdar E. Facile fabrication and characterization of modified spray deposited cadmium sulphide thin films. Physica B: Condensed Matter. 2019;571:64-70.
39. Dabhane H, Ghotekar S, Tambade P, Pansambal S, Murthy HA, Oza R, et al. A review on environmentally benevolent synthesis of CdS nanoparticle and their applications. Environmental Chemistry and Ecotoxicology. 2021;3:209-19.
40. Patra P, Kumar R, Kumar C, Mahato PK. Ni-incorporated cadmium sulphide quantum dots for solar cell: An evolution to microstructural and linear-nonlinear optical properties. Journal of Crystal Growth. 2022:126542.
41. Munyai S, Hintsho-Mbita N. Green derived metal sulphides as photocatalysts for waste water treatment. A review. Current Research in Green and Sustainable Chemistry. 2021;4:100163.
42. Zhang J, Wageh S, Al-Ghamdi A, Yu J. New understanding on the different photocatalytic activity of wurtzite and zinc-blende CdS. Applied Catalysis B: Environmental. 2016;192:101-7.
43. Zhang QL, Ji ZJ, Zhou J, Zhao XC, Lan XZ. Preparation of Lanthanum Oxide Nanoparticles by Chemical Precipitation Method. Materials Science Forum. 2012;724:233-6.
44. Josephine DSR, Sakthivel B, Sethuraman K, Dhakshinamoorthy A. Synthesis, Characterization and Catalytic Activity of CdS-Graphene Oxide Nanocomposites. ChemistrySelect. 2016;1(10):2332-40.
45. Abdelghany A, Abdelrazek E, Rashad D. Impact of in situ preparation of CdS filled PVP nano-composite. Spectrochimica Acta Part A: Molecular and Biomolecular Spectroscopy. 2014;130:302-8.
46. Yang J, Xie T, Zhu Q, Wang J, Xu L, Liu C. Boosting the photocatalytic activity of BiOX under solar light via selective crystal facet growth. Journal of Materials Chemistry C. 2020;8(7):2579-88.
47. Voronova M, Rubleva N, Kochkina N, Afineevskii A, Zakharov A, Surov O. Preparation and characterization of polyvinylpyrrolidone/cellulose nanocrystals composites. Nanomaterials. 2018;8(12):1011.
48. Elfeky AS, Salem SS, Elzaref AS, Owda ME, Eladawy HA, Saeed AM, et al. Multifunctional cellulose nanocrystal/metal oxide hybrid, photo-degradation, antibacterial and larvicidal activities. Carbohydrate polymers. 2020;230:115711.

49. Miao C, Hamad WY. Critical insights into the reinforcement potential of cellulose nanocrystals in polymer nanocomposites. Current Opinion in Solid State and Materials Science. 2019;23(4):100761.
50. Huang S, Zhou L, Li M-C, Wu Q, Kojima Y, Zhou D. Preparation and properties of electrospun poly (vinyl pyrrolidone)/cellulose nanocrystal/silver nanoparticle composite fibers. Materials. 2016;9(7):523.
51. Bühler V. Polyvinylpyrrolidone excipients for pharmaceuticals: povidone, crospovidone and copovidone. 1 ed: Springer Science & Business Media; 2005.
52. Bhatia D, Mittal A, Malik DK. Antimicrobial activity of PVP coated silver nanoparticles synthesized by Lysinibacillus varians. 3 Biotech. 2016;6(2):1-8.
53. Kobeissi JM, Hassan GF, Karam P. Silver-modified cross-linked polyvinylpyrrolidone and its antibacterial activity. ACS Applied Bio Materials. 2018;1(6):1864-70.
54. Ushiyama F, Amada H, Takeuchi T, Tanaka-Yamamoto N, Kanazawa H, Nakano K, et al. Lead identification of 8-(methylamino)-2-oxo-1, 2-dihydroquinoline derivatives as DNA gyrase inhibitors: hit-to-lead generation involving thermodynamic evaluation. ACS omega. 2020;5(17):10145-59.
55. Schiebel J, Chang A, Shah S, Lu Y, Liu L, Pan P, et al. Rational design of broad spectrum antibacterial activity based on a clinically relevant enoyl-acyl carrier protein (ACP) reductase inhibitor. Journal of Biological Chemistry. 2014;289(23):15987-6005.
56. Abagyan R, Totrov M. Biased probability Monte Carlo conformational searches and electrostatic calculations for peptides and proteins. Journal of molecular biology. 1994;235(3):983-1002.
57. Zhou R-H, Wei Z-H, Li Y-Y, Li Z-J, Yao H-C. Construction of visible light–responsive Z-scheme CdS/BiOI photocatalyst with enhanced photocatalytic CO2 reduction activity. Journal of Materials Research. 2019;34(23):3907-17.
58. Arularasu M, Harb M, Sundaram R. Synthesis and characterization of cellulose/TiO2 nanocomposite: Evaluation of in vitro antibacterial and in silico molecular docking studies. Carbohydrate Polymers. 2020;249:116868.
59. Susha N, Nandakumar K, Nair SS. Enhanced photoconductivity in CdS/betanin composite nanostructures. RSC advances. 2018;8(21):11330-7.
60. Manikandan K, Dilip CS, Mani P, Prince JJ. Deposition and characterization of CdS nano thin film with complexing agent triethanolamine. American Journal of Engineering and Applied Sciences. 2015;8(3):318.
61. Rao GT, Babu B, Stella RJ, Manjari VP, Reddy CV, Shim J, et al. Synthesis and characterization of VO2+ doped ZnO–CdS composite nanopowder. Journal of Molecular Structure. 2015;1081:254-9.
62. El-Sadek A, Wasly H, Batoo KM. X-ray peak profile analysis and optical properties of CdS nanoparticles synthesized via the hydrothermal method. Applied Physics A. 2019;125(4):1-17.
63. Shivashankarappa A, Sanjay K. Study on biological synthesis of cadmium sulfide nanoparticles by Bacillus licheniformis and its antimicrobial properties against food borne pathogens. Nanoscience and Nanotechnology Research. 2015;3(1):6-15.
64. Elfalaky A, Mansur A, Maged FA. Polyaniline-CdSNanocomposite; Synthesis, Structural, Thermal and Spectroscopic Analysis. IOSR J Appl Phys (IOSR-JAP). 2015;7(3):92-100.
65. Li W, Cai G, Zhang P. A simple and rapid Fourier transform infrared method for the determination of the degree of acetyl substitution of cellulose nanocrystals. Journal of Materials Science. 2019;54(10):8047-56.
66. Abidi N, Cabrales L, Haigler CH. Changes in the cell wall and cellulose content of developing cotton fibers investigated by FTIR spectroscopy. Carbohydrate Polymers. 2014;100:9-16.
67. Su FY, Xu CQ, Yu YX, Zhang WD. Carbon Self-Doping Induced Activation of n–π* Electronic Transitions of g-C3N4 Nanosheets for Efficient Photocatalytic H2 Evolution. ChemCatChem. 2016;8(22):3527-35.

68. Jothi NN, Christy PD, Suganthi AB, Ramalingam G, Sagayaraj P. Development of CdS nanorods of high aspect ratio under hydrothermal conditions with PEG template. Journal of Crystal Growth. 2011;316(1):126-31.
69. Kandi D, Behera A, Martha S, Naik B, Parida K. Quantum confinement chemistry of CdS QDs plus hot electron of Au over TiO2 nanowire protruding to be encouraging photocatalyst towards nitrophenol conversion and ciprofloxacin degradation. Journal of Environmental Chemical Engineering. 2019;7(1):102821.
70. Berestennikov A, Li Y, Iorsh I, Zakhidov AA, Rogach A, Makarov S. Beyond quantum confinement: excitonic nonlocality in halide perovskite nanoparticles with Mie resonances. Nanoscale. 2019;11(14):6747-54.
71. Shkir M, Anis M, Shaikh S, AlFaify S. An investigation on structural, morphological, optical and third order nonlinear properties of facilely spray pyrolysis fabricated In: CdS thin films. Superlattices and Microstructures. 2019;133:106202.
72. Teodorescu M, Bercea M. Poly (vinylpyrrolidone)–a versatile polymer for biomedical and beyond medical applications. Polymer-Plastics Technology and Engineering. 2015;54(9):923-43.
73. Singer A, Barakat Z, Mohapatra S, Mohapatra SS. Chapter 13 - Nanoscale Drug-Delivery Systems: In Vitro and In Vivo Characterization. In: Mohapatra SS, Ranjan S, Dasgupta N, Mishra RK, Thomas S, editors. Nanocarriers for Drug Delivery: Elsevier; 2019. p. 395-419.
74. Henry F, Marchal P, Bouillard J, Vignes A, Dufaud O, Perrin L, editors. The effect of agglomeration on the emission of particles from nanopowders flow. 14 International Symposium on Loss Prevention and Safety Promotion in the Process Industry; 2013: Citeseer.
75. Naz M, Rafiq A, Ikram M, Haider A, Ahmad SOA, Haider J, et al. Elimination of dyes by catalytic reduction in the absence of light: A review. Journal of Materials Science. 2021;56(28):15572-608.
76. Raza A, Hassan J, Ikram M, Naz S, Haider A, Ul-Hamid A, et al. Molecular docking and DFT analyses of magnetic cobalt doped MoS2 and BN nanocomposites for catalytic and antimicrobial explorations. Surfaces and Interfaces. 2021;27:101571.
77. Ikram M, Tabassum R, Qumar U, Ali S, Ul-Hamid A, Haider A, et al. Promising performance of chemically exfoliated Zr-doped MoS 2 nanosheets for catalytic and antibacterial applications. RSC Advances. 2020;10(35):20559-71.
78. Nguyen Thi Thu T, Nguyen Thi N, Tran Quang V, Nguyen Hong K, Nguyen Minh T, Le Thi Hoai N. Synthesis, characterisation, and effect of pH on degradation of dyes of copper-doped TiO2. Journal of Experimental Nanoscience. 2016;11(3):226-38.
79. Ikram M, Hayat S, Imran M, Haider A, Naz S, Ul-Hamid A, et al. Novel Ag/cellulose-doped CeO2 quantum dots for efficient dye degradation and bactericidal activity with molecular docking study. Carbohydrate polymers. 2021;269:118346.
80. Mostafa AM, Mwafy EA, Hasanin MS. One-pot synthesis of nanostructured CdS, CuS, and SnS by pulsed laser ablation in liquid environment and their antimicrobial activity. Optics & Laser Technology. 2020;121:105824.
81. Goy RC, Morais ST, Assis OB. Evaluation of the antimicrobial activity of chitosan and its quaternized derivative on E. coli and S. aureus growth. Revista Brasileira de Farmacognosia. 2016;26:122-7.
82. Malarkodi C, Rajeshkumar S, Paulkumar K, Vanaja M, Gnanajobitha G, Annadurai G. Biosynthesis and Antimicrobial Activity of Semiconductor Nanoparticles against Oral Pathogens. Bioinorganic Chemistry and Applications. 2014;2014:347167.
83. Rajendiran K, Zhao Z, Pei D-S, Fu A. Antimicrobial activity and mechanism of functionalized quantum dots. Polymers. 2019;11(10):1670.

84. Haider A, Ijaz M, Imran M, Naz M, Majeed H, Khan J, et al. Enhanced bactericidal action and dye degradation of spicy roots' extract-incorporated fine-tuned metal oxide nanoparticles. Applied Nanoscience. 2020;10(4):1095-104.
85. Naz S, Ngo T, Farooq U, Abagyan R. Analysis of drug binding pockets and repurposing opportunities for twelve essential enzymes of ESKAPE pathogens. PeerJ. 2017;5:e3765.
86. Lu H, Tonge PJ. Inhibitors of FabI, an enzyme drug target in the bacterial fatty acid biosynthesis pathway. Accounts of chemical research. 2008;41(1):11-20.
87. Collin F, Karkare S, Maxwell A. Exploiting bacterial DNA gyrase as a drug target: current state and perspectives. Applied microbiology and biotechnology. 2011;92(3):479-97.
88. Haque M, Lyndem S, Singha Roy A. Interaction Properties of Biosynthesized Cadmium Sulphide Quantum Dots with Human Serum Albumin: Further Investigation of Antibacterial Activities and Sensing Applications. Luminescence. 2022.
89. Singh IR, Chettri U, Maity P, Ghosh AK, Joshi S, Mitra S. Modulated Antimicrobial Activity and Drug-Protein Interaction Ability of Zinc Oxide and Cadmium Sulfide Nanoparticles: Effect of Doping with Few First-Row Transition Metals. Journal of Cluster Science. 2022:1-13.
90. Shivashankarappa A, Sanjay KR. Escherichia coli-based synthesis of cadmium sulfide nanoparticles, characterization, antimicrobial and cytotoxicity studies. Brazilian Journal of Microbiology. 2020;51(3):939-48.

Abstract

In present study, control sized cadmium sulphide (CdS) quantum dots (QDs) and cellulose nanocrystals grafted polyvinylpyrrolidone (CNC-g-PVP) doped CdS QDs were synthesized via co-precipitation. The suggested pathway is fruitful in throwing out organic pollutants like methylene blue (MB) from industrial water and bactericidal applications. A series of characterization techniques were used to determine the structural, optical and morphological qualities of prepared samples. The X-ray diffraction (XRD) pattern verified hexagonal structure with no significant change occurring in the spectrum upon doping (2, 4, and 6%). The UV-vis spectrophotometer describes blueshift in absorption pattern, resulting in an increase in band gap energy (E_g) upon doping. Catalytic activity (CA) against MB in basic and neutral medium demonstrated remarkable results compared with the acidic medium. Furthermore, bactericidal potential of doped sample (6%) exhibited the significantly higher inhibition zones of 5.25 mm and 4.05 mm against Staphylococcus aureus (*S. aureus)* or Gram-positive (G_+ve) *and* Escherichia coli *(E. coli)* or Gram-negative (G-ve), respectively. *In silico* predictions for these doped QDs were performed against selected enzyme targets (i.e. DNA gyrase and FabI) to unveil the mystery governing these bactericidal activities.